Schweizerische Eidgenossenschaft
Confédération suisse
Confederazione Svizzera
Confederaziun svizra

Eidgenössisches Departement für
Umwelt, Verkehr, Energie und Kommunikation UVEK

Bundesamt für Energie BFE

Schlussbericht 10. August 2014

Petrophysical and geophysical field study of a fossilized hydrogeothermal system in Geitafell, Iceland

Master Thesis

Auftraggeber:

Bundesamt für Energie BFE
Forschungsprogramm Geothermie
CH-3003 Bern
www.bfe.admin.ch

Auftragnehmer:

Department of Earth Science
ETH Zurich, 8092 Zurich, Switzerland
http://www.erdw.ethz.ch

Autoren:

Zuercher Benjamin, ETHZ, zuercheb@student.ethz.ch
Co-Autor: Stewart Greenhalgh, Institute of Geophysics, ETH Zurich

BFE-Bereichsleiter: Gunter Siddiqi
BFE-Programmleiter: Rudolf Minder
BFE-Vertragsnummer: SI/500913-01

Petrophysical and geophysical field study of a fossilised hydrogeothermal system in Geitafell, Iceland

Master-thesis

August 10, 2014

Zuercher Benjamin, zuercheb@student.ethz.ch

Main Supervisor: Prof. Dr. Stewart Greenhalgh, Institute of Geophysics, ETH Zurich
Co-Referee: Dr. Benoît Cordonnier, Institute of Geology, ETH Zurich
Add. Supervisor: Prof. Dr. Hansrudolf Maurer, Institute of Geophysics, ETH Zurich

Department of Earth Sciences, ETH Zurich

ETH
Eidgenössische Technische Hochschule Zürich
Swiss Federal Institute of Technology Zurich

DERDW
Department of Earth Sciences

Abstract

This MSc-thesis project is an investigation of petrophysical properties of a fossilised high-temperature hydrogeothermal system in Geitafell in the south-east of Iceland. It involved both laboratory determinations of elastic properties on small samples as well as in-situ measured seismic and electrical properties. The objective was to get actual field values on three profiles which started in intrusive material (old magma chamber, gabbro), continued to the transition zone (hornfels) and ended in the altered host rock (basalt) which was intersected by a decreasing number of dykes and sheets towards the end of the lines. Three other lines were chosen to yield information about the variations (different degrees of alteration) in the host rock. Data quality for all measurements was moderate (mainly due to poor contact between geophones/electrodes and the ground). Data pre-processing and inverse modeling were used to turn the measured data into the most reasonable images of subsurface structure. A high smoothing factor was applied to counter the under-determination nature of the inverse problem. The seismic arrival times needed to be corrected for static shift. As a result, ranges of P-wave velocities and resistivities could be extracted from subsurface models on the basis of several defined criteria. The P-wave velocities measured in the field were then compared to P-wave velocities at various pressures measured in the Rock Physics lab at ETH Zurich. These rock samples were collected from the field site in Geitafell and geochemical analysis showed that the differences in composition were minor. The determined velocities for both measurements are in good agreement with each other and the rather high velocity values can be attributed to low porosity. The small differences between the field and lab velocities can be explained by the different frequencies and length scales used in the measurements.

Contents

List of Figures

List of Tables

1 Introduction

Since the Swiss Government has decided to discontinue its nuclear energy program and because of the increasing societal demand for new sources of clean energy, it is essential to develop and apply geophysical techniques to explore and characterise geothermal reservoirs. This will provide a better understanding of the potential future energy supplies. Therefore research on the petrophysical properties of the subsurface of hydrogeothermal systems is of high interest and provided the motivation for the present study.

1.1 Geothermal systems in Iceland

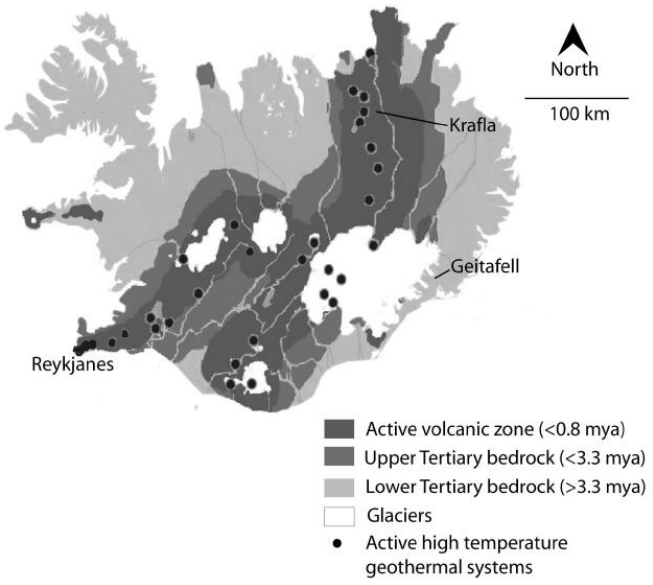

Figure 1: Map of Iceland with locations of studied hydrothermal systems. Krafla and Reykjanes represent an active system, while Geitafell in South-East Iceland is a fossilised one. The map is copied from [Elders, 2010].

Geothermal systems in Iceland can be broadly classified into three categories: high-temperature active systems, low-temperature systems and fossilised high-temperature systems which occur in Quaternary and Tertiary formations [Arnórsson, 1995]. They are shown in Figure 1. The reason for their existence and geographic expression is a mantle plume beneath Iceland and the diverging European and American lithospheric plates

[Arnórsson, 1995]. This rifting has let to an increased temperature gradient [Arnórsson, 1995]. New crust is formed in the center of this rifting, while older rock material (oldest rocks date back to 15-17 m.y.) becomes more eroded with increasing distance from the rifting zone [Franzson et al., 2001]. Most rocks are of basaltic composition but with a few exceptions andesitic and rhyolitic rocks are also found [Franzson et al., 2001]. Both sub-aerial and sub-glacial lava occur in large volumes, while sedimentary rock deposits are only minor and found where erosional processes are active [Franzson et al., 2001].
The rocks of high-temperature areas are geologically very young and permeable [Arnórsson, 1995] and consist of basaltic lava series intervened by hyaloclastites [Franzson et al., 2001]. More intrusive rocks in the form of sheets and dykes become more common at deeper levels [Franzson et al., 2001]. Figure 2 is a schematic diagram showing all involved rocks in a high-temperature system such as at Iceland.

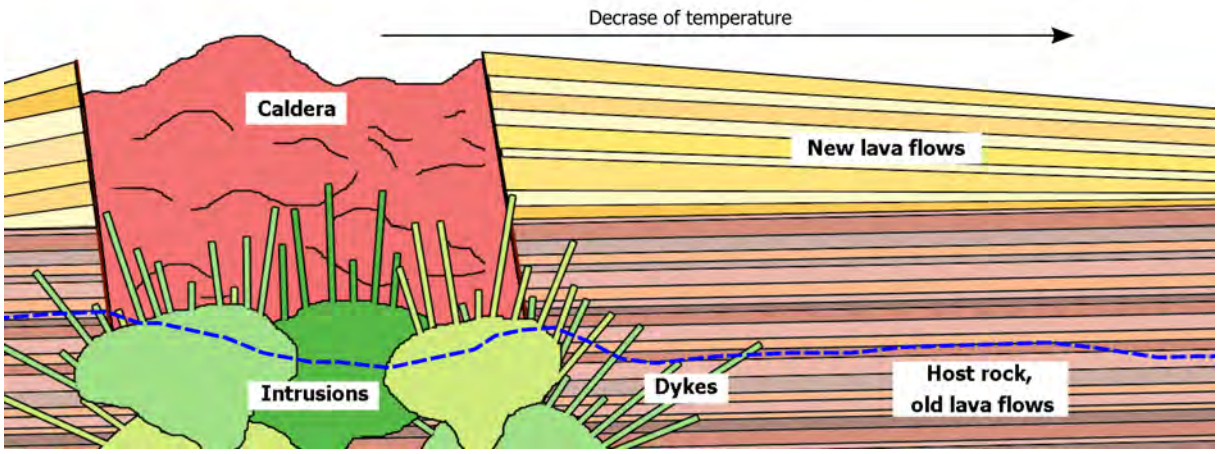

Figure 2: Schematic Figure of a high-temperature system. The caldera is surrounded by host rock (basalt) and new lava flows, while intrusions and dykes occur periodically over the active time of the system. The thickness of lava flows can vary as well as their chemical composition. Temperature decreases with increasing distance from the caldera but each system has its own individual maximum temperature. Intruded dykes can increase the temperature locally for a certain period of time. The blue dotted line shows a possible erosion horizon of a future fossilised system [Grab, 2014].

The water cycle of a natural hydrogeothermal system is driven by a heat source (solidification and cooling of magma intrusives) and its natural recharge is cold rainwater and groundwater from the vicinity [Arnórsson, 1995], as shown in Figure 3. The reservoir temperature is then a combined effect of the groundwater flow and the rate of heat transfer from the heat source to the water [Arnórsson, 1995].

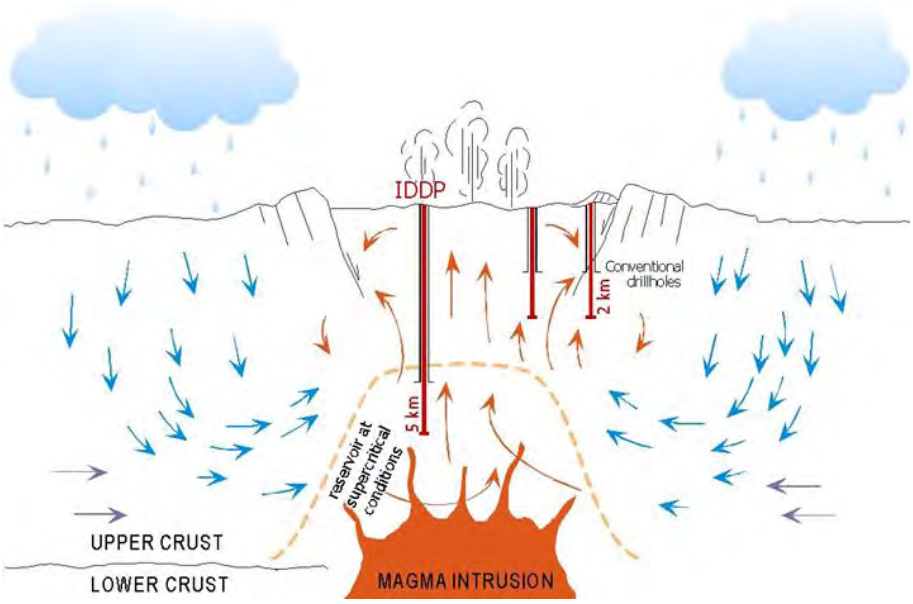

Figure 3: Schematic model cross section of a high-temperature geothermal system in Iceland including the targeted area of the IDDP project, where the reservoir has supercritical conditions, [Elders and Fridleifsson, 2010].

Fossilised or extinct high-temperature geothermal systems are associated with a central volcanic complex, which was then partly eroded, hence the inner structures such as cone sheets and dykes are exposed at the surface [Arnórsson, 1995, Fridleifsson, 1983a,b]. This is shown by the blue dotted line in Figure 2. The rocks exhibit evidence of hydrothermal alteration [Arnórsson, 1995, Fridleifsson, 1983a,b]. This complex process is an interaction of thermal fluids with rocks controlled by permeability and temperature [Franzson et al., 2001]. The primary constituents of volcanic rocks are replaced by temperature-typical alteration minerals [Franzson et al., 2001]. These geothermal systems show then a depth-zonal distribution of secondary minerals [Arnórsson, 1995, Fridleifsson, 1983a,b].

1.2 The COTHERM project

A research project called COTHERM (COmbined hydrological, geochemical and geophysical modeling of geoTHERMal systems) funded by the Swiss National Science Fundation, was launched in 2012 for a better understanding of magmatically-driven subsurface processes in natural geothermal systems [Driesner, 2012]. It is a synergistic project linking hydro-thermal modeling with fluid-rock chemical interaction modeling, geophysical simulation and ground truthing from field studies in Iceland.

The IDDP (Icelandic Deep Driling Project) is seeking to drill into deeper zones (see Figure 3) where supercritical fluids occur instead of drilling conventional geothermal wells that produce a mixture of steam and water. The pressure enthalpy diagram for water is shown in Figure 4 [Elders and Fridleifsson, 2010] and illustrates the point. This should increase the enthalpy of the production well enormously, hence a lot more electrical energy can be produced [Elders and Fridleifsson, 2010]. Because of unsuccessful first attempts [Elders and Fridleifsson, 2010] more projects such as the EU-funded IMAGE (Integrated Methods for Advanced Geothermal Exploration) project have been initiated to get more accurate information about the physical and chemical properties of the contact zone in a fossilised high-temperature hydrogeothermal system.

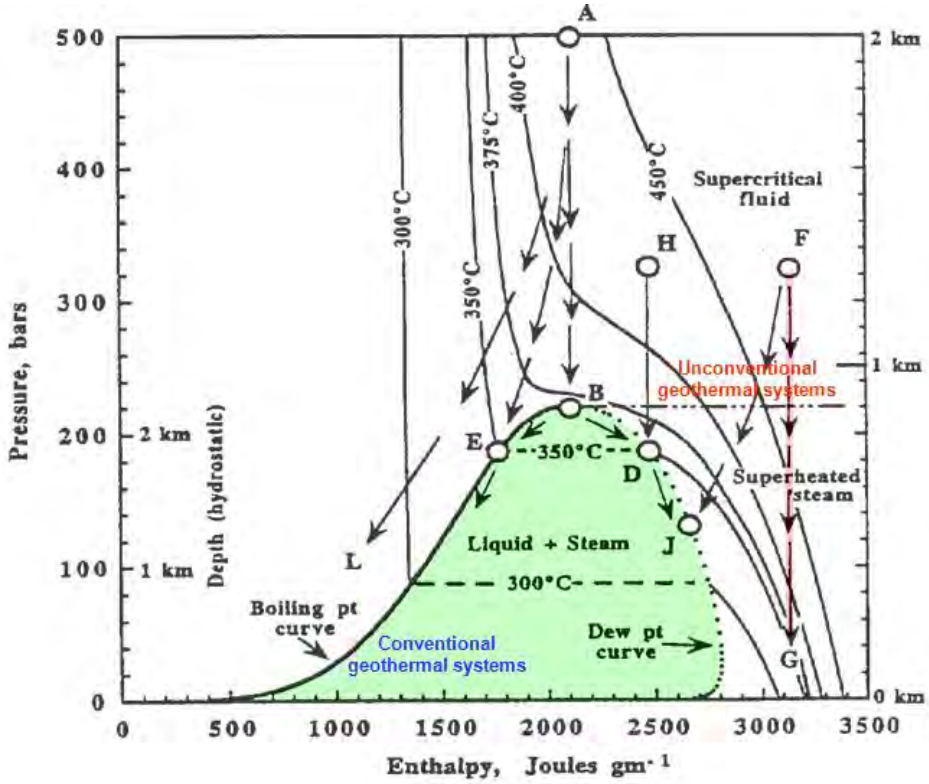

Figure 4: Pressure enthalpy diagram for pure water. Unconventional geothermal systems have much higher enthalpies than the conventional ones and act with supercritical fluid and superheated steam instead of liquid and steam [Elders and Fridleifsson, 2010].

1.3 Previous investigations

The use and interpretation of geophysical measurements is an important way to identify and characterise geothermal systems because the subsurface shows inhomogeneities in the physical properties (density, elasticity, electrical resistivity, etc.). These are highly affected by the local pressure, temperature and fluid content conditions. Viewed from the geological perspective, factors such as rock type, porosity, fracturing, cementation and many others influence the physical rock properties. Small-scale features can be resolved at shallow depths, but not the actual target at greater depths [Driesner, 2012].

1.3.1 Petrophysical lab measurements of basaltic rocks

Laboratory studies on the electrical properties of Icelandic rocks were carried out by Flóvenz et al. [2005] and Kulenkampff et al. [2005], in which the conductivity of altered (smectite, chlorite) basaltic rocks were measured and the dependence on temperature and pressure were analysed.
Comparable measurements of basaltic rock samples from the upper crust of high temperature areas but not from deeper parts were carried out by Kristinsdóttir et al. [2010] and Jaya et al. [2010]. They obtained precise results on both electrical resistivity and P-wave velocity and their dependence on temperature.
Laboratory determinations of seismic velocities and fluid permeability on lava flow from Etna were reported by Fortin et al. [2011] who could show that the velocity increases with increasing hydrostatic pressure due to the closure of the pre-existing thermal cracks.
Madonna and Tisato [2013] tested a new seismic wave attenuation module in the laboratory which can measure the attenuation at low frequencies.
An investigation on Icelandic basaltic rock samples was performed by Adelinet et al. [2010] to distinguish differences in elastic properties during measurements with low and high frequencies in dry and saturated conditions, respectively. These experiments give a first approach of how to deal with the problem of comparing field data (LF) and lab data (HF).
Due to the lack of knowledge of physical rock properties in the lower crust in Iceland, rock samples from all over Iceland were collected at the surface and are expected to be equivalent to those from a geothermal reservoir [Franzson et al., 2001]. Our study is based on a similar approach. The analysis by Franzson et al. [2001] indicated that the rock alteration in basaltic lavas is related to the primary porosity of the rock. Grain density

first decreases with increasing alteration. Grain density increases then for much higher temperatures due to the formation of higher density alteration minerals [Franzson et al., 2001].
General petrophysical findings and models for elasticity and seismic velocity are listed in the book by Mavko et al. [2009].

1.3.2 Geophysical field measurements

The broad lithospheric structure of Iceland is fairly well known, mainly from refraction profiles as well as P and S wave travel times from microearthquakes [Menke et al., 1998]. The crust is generally 25 to 31 km thick but also structures such as high-velocity domes from central volcanos have been delineated [Menke et al., 1998]. The 3-D velocity structures has been deduced to depths of 10-15 km in the southwest of Iceland where local structures such as the Hengill central volcano were delineated [Tryggvason et al., 2002]. Reduced wavespeeds were interpreted as supercritical fluids within the volcanic fissure system [Tryggvason et al., 2002].
In addition to the seismic analyses of the subsurface in Iceland, extensive studies of resistivity structures have been made in active volcano areas. Shallow conductive layers were found from transient electromagnetic (TEM) and magnetotelluric (MT) measurements which can be explained by the presence of alteration minerals [Árnason et al., 2010]. This low resistivity structure at the outer margin of the reservoir is typically underlain by a more resistive core towards the inner part where less conductive alteration minerals are present [Árnason et al., 2000]. Hence resistivity values can also be used as a thermometre [Árnason et al., 2000].
More focused geophysical field measurements have been conducted to characterise the subsurface of Iceland, mostly across active zones e.g. Eysteinsson and Hermance [1985], Hersir et al. [1984], Planke et al. [1999] and to correlate different data types e. g. Hermance and Grillot [1970]. Magnetic properties of rocks from the Geitafell gabbro complex were also investigated [Schoenharting, 1979].
How a difficult and complex terrain can affect geophysical field measurements and some ideas on how to avoid problems is well described by Maurer and Hauck [2007], in the context of elucidating on alpine rock glacier.

1.4 Aims of MSc-thesis

To learn more about the properties of a fossilised high-temperature system (Geitafell) two MSc projects forming a combined geophysical and geochemical study were undertaken within COTHERM. They began in summer 2013, with the objective to perform a detailed geochemical characterization (exact mineralogy) of several outcrops and complementary to this, a geophysical study (field and lab measurements) was carried out in the same area. The primary purpose was to better understand how geophysical signals on various scales can be interpreted in terms of actual geology in a geothermal context.
In this thesis, the specific aim was to determine the petrophysical properties of representative lithological units in a fossilised hydrogeothermal system. Seismic and DC electric field data, targeting the first few tens of metres, were recorded to yield information about the seismic velocities and resistivities of the subsurface.
One important question is whether the body shape of the old magma chamber be partially reconstructed from such measurements? Another related question is how do physical properties of rocks change in a fossilised hydrothermal system when moving further away from the old heat source (old magma chamber) of the circulating water? I wish to ascertain whether lower ambient rock temperature during the active stage of the hydrothermal system (and therefore a slightly different chemical composition) have any affect on the physical rock properties.
The success of the investigation depends mostly on the quality of the field data.
Representative rock samples were collected from the field and then analysed in the Rock Physics lab at ETH. Hence, a comparison of field and lab data of seismic velocities can be made. But this needs to be done carefully due to the different length scales and different frequencies used in the field and in the lab measurements.
My MSc-thesis project should support the geophysical modeling part of the COTHERM project with actual field data of a fossilised system (Geitafell) to enhance the synthetic geophysical modelling of an active system, and related studies on synthetic data inversions.

1.5 Thesis outline

Chapter 2 gives an overview of the local geology of the study site in Iceland. Field work and all chosen profile lines (in relation to the geology) are also detailed in this chapter. The basic principles of the methods used are described in Chapter 3. They cover seismic refraction tomography, electrical resistivity tomography and seismic velocity determinations. This chapter deals also with the data processing techniques employed. The reconstructed subsurface models are presented and described in Chapter 4. Chapter 5 is a Discussion chapter. It includes the quality of the measured data as well as comparisons with petrophysical lab data and relationships to geochemical and physical properties. In chapter 6, I present Conclusions for the study and an Outlook for future work.

2 Study Site

Fridleifsson [1983a] undertook a large-scale geological analysis of the Geitafell central complex (see appendix A, Figure 42). It is therefore opportune to perform further geophysical investigations to learn more about the petrophysical properties (resistivities, seismic velocities) of the rocks involved in a hydrogeothermal system.

2.1 Geology

Geitafell volcano complex in South-East Iceland (see Figure 1) is a fossilised high temperature hydrogeothermal system (today deeply eroded) which was driven by a magmatic heat source [Fridleifsson, 1983a, 1986, Burchardt and Gudmundsson, 2009, Burchardt et al., 2011, Arnórsson, 1995]. The lifetime of this system has been estimated to be between 200'000 and 300'000 years some 5 to 6 m. y. ago, so intrusions may have been occurred periodically over this time [Fridleifsson, 1983a, 1986, Burchardt and Gudmundsson, 2009, Burchardt et al., 2011]. Figure 5 shows the study site including the parts of the high-temperature system that still can be found after the erosion caused by the nearby glacier (Hoffellsjokull).

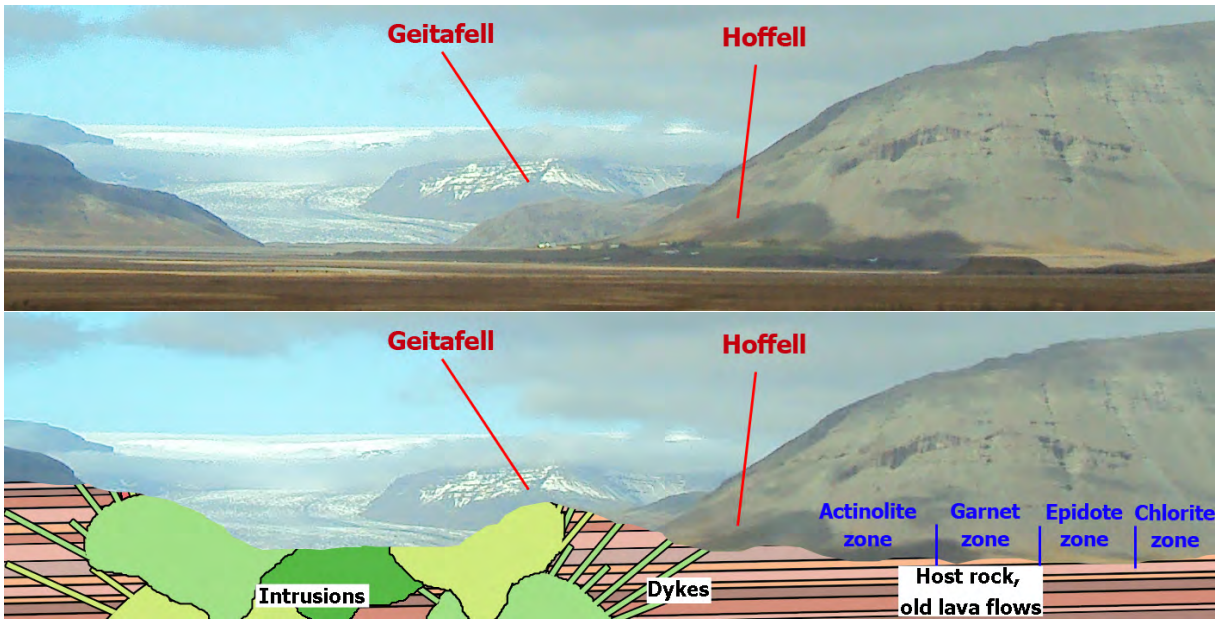

Figure 5: Study site in the south-east of Iceland including a schematic diagram of an eroded fossilised high-temperature system. Geophysical measurements were carried out at Geitafell and Hoffell. The borders of the alteration zones are only drawn schematically and are not at the exact location. The intrusion density decreases with distance away from the old magma chamber [Grab, 2014].

The Gabbro (intrusive body) is estimated to have a thickness of 0.5 km and to cover an area of 1 x 2.5 km and was located at 1 km depth below the ground surface [Fridleifsson, 1983a, 1984, 1986]. The initial temperature was assumed to be 1225 °C and the average temperature of the host rock between 125 °C and 225 °C, hence the thermal gradient was between 100 ° C/km and 180 ° C/km [Fridleifsson, 1983a, 1986]. These values were derived from mineral deposits within the gabbro and host rock [Fridleifsson, 1983a, 1986]. Seven mineral vein systems and twelve intrusive phases were found in the Geitafell volcanic system including their time relation [Fridleifsson, 1983a,b]. The mineralogical evidence suggests that supercritical and superheated fluid layers may have existed in the hydrothermal system [Fridleifsson, 1983a,b, 1986]. Furthermore, four mineral zones (secondary minerals: chlorite, epidote, garnet and actinolite; they indicate different temperature conditions) appear in the host rock [Fridleifsson, 1983a,b, 1986]. They were mapped by Fridleifsson [1983a] and can be found in Appendix B, Figure 43. Chlorite appears above a temperature of 100 °C, epidote above about 200 °C and garnet and actinolite are high temperature alteration minerals (∼300 °C) [Henley and Ellis, 1983, Lagat, 2007]. These minerals and other typical alteration minerals are shown in Figure 6, along with their temperature range. It shows what temperature the system needs to be for a certain mineral to form, hence these minerals can be used as a thermometre for the past.

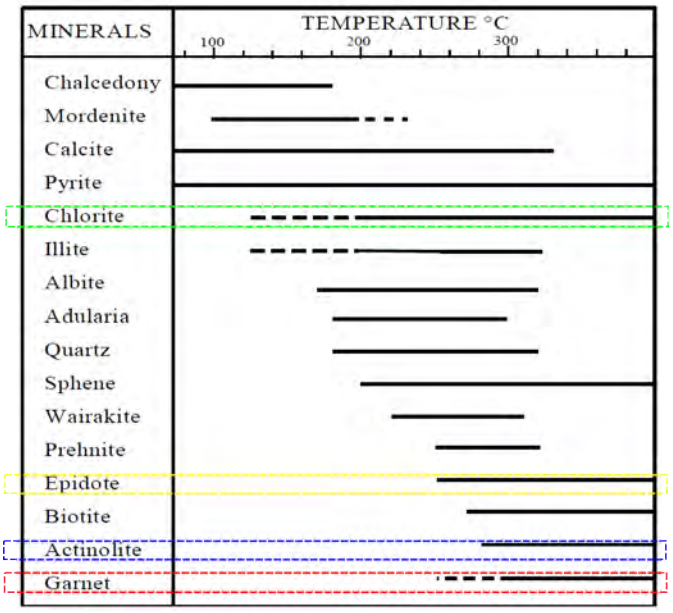

Figure 6: Alteration minerals plotted as a function of temperature. The main alteration minerals found in Hoffell are highlighted (Figure copied from [Lagat, 2007]).

For simplification purposes the following classification of rock types was used in the pre-study (mapping) for the later geophysical measurements:

- gabbro
- dyke/sheet (basalt/dolerite/dolerite porphyric/rhyolite)
- hornfels
- basalt (host rock, with or without vesicles + actinolite/garnet/epidote/chlorite)
- rhyolite

Gabbro can be seen as the old magma chamber and dykes and sheets as intrusions into the host rock which comprises basalt (see Figure 7). Dykes, sheets and also the host rock can vary a lot, hence several sub-classifications were used. Hornfels is the result of heated host rock due to contact metamorphism and can normally found close to the contact zone between the old magma chamber and the surrounding rocks. Rhyolitic material can only be found in minor amounts, therefore it is not as important as the others but still worth mentioning.

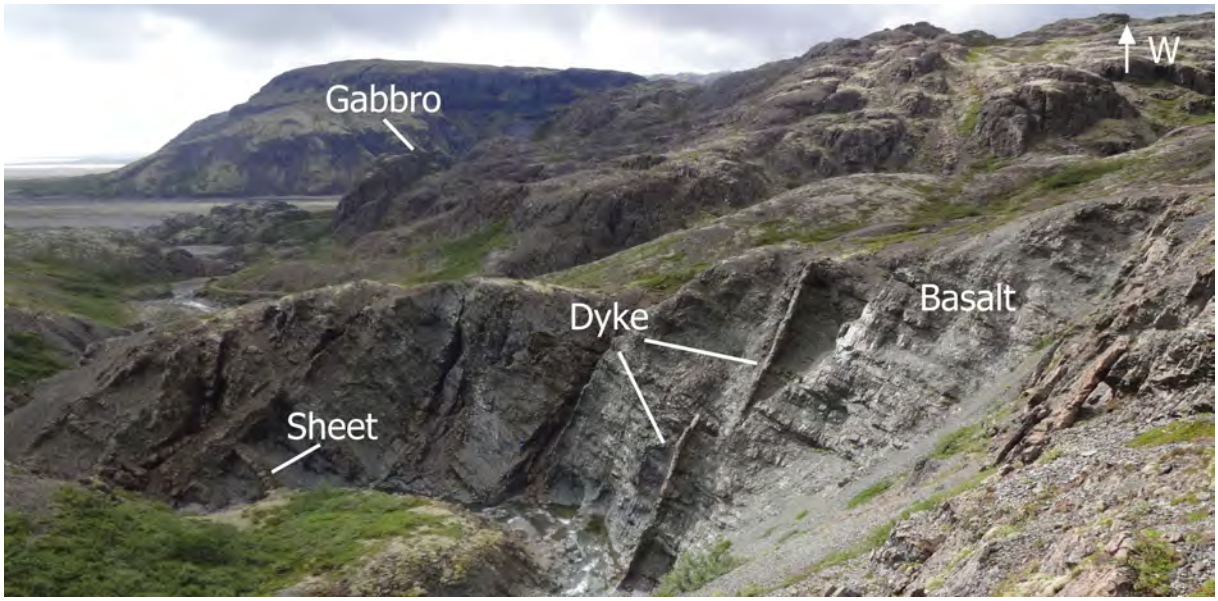

Figure 7: Photograph of sheets and dykes at eroded Geitafell volcano complex surrounded by basalt (host rock). Gabbro (old magma chamber) can be found in the back, hence the view is from the outside of the old magma chamber into it. The closer to the gabbro, the more sheets and dykes can be found.

2.2 Field work

Geophysical field data acquisition was carried out in September 2013 and was an essential component of this thesis research. I was specifically interested in determine seismic wavespeeds and resistivities of the involved rocks in a hydrogeothermal system. Hence a geological pre-study was essential. Omar Fridleifsson's PhD-thesis with all his geological mapping (see the Appendix, Figure 42 and 43) was used as a basis for further mapping by ourselves. Additionally, we were given a geological introduction directly in the field by Omar Fridleifsson. We concentrated afterwards on localizing the exact transition of gabbro and basalt at several chosen places where field measurements were considered as to be plausible practicable. The resultant map which shows the geology is given as Figure 8. All this geological field work was conducted in August 2013, including a lot of small-scale geological mapping from the other MSc-project.

The mapped transitions let us define a starting point of the profile lines which we wanted to measure afterwards. We decided to measure at three sites (A, B, C) in Geitafell (see Figure 9) to obtain several results close to the contact. The main interest was to image the first few tens of metres on a line starting from the old magma chamber (gabbro), going to the transition zone where we expect hornfels (just a few metres thick) and then finishing in basaltic hostrock with a decreasing number of dykes towards the last measuring point of the line. We also wanted to learn more about the relation between the physical properties of the rocks and their alteration at three sites (X, Y, Z) in Hoffell (see Figure 9). The slightly different chemical composition and the change in grain size has an affect on the petrophysical properties. But there is to suggestion that these variations are very small and it was not clear that they could be detected from geophysical field measurements.

In summary, we made measurements at six locations (seismic and DC electric measurements) during our geophysical field campaign in September 2013. The exact locations are shown in Figure 9. A two metre spacing for both geophones and electrodes was applied in the field. This distance was chosen as a compromise to gain a good enough resolution but also to reach a penetration depth of several tens of metres. All station positions were surveyed by means of GPS. A multi-electrode system (Syscal or Geotom) was used in the field to measure rock resistivities and a shotgun or a hammer was used for the seismic source. A more detailed list of recording parametres can be found in chapter 3, in the subsection on recording parametres.

Besides these field measurements, rock samples from each litholocigal unit were collected for further investigations in the Rock Physics Lab at ETH.

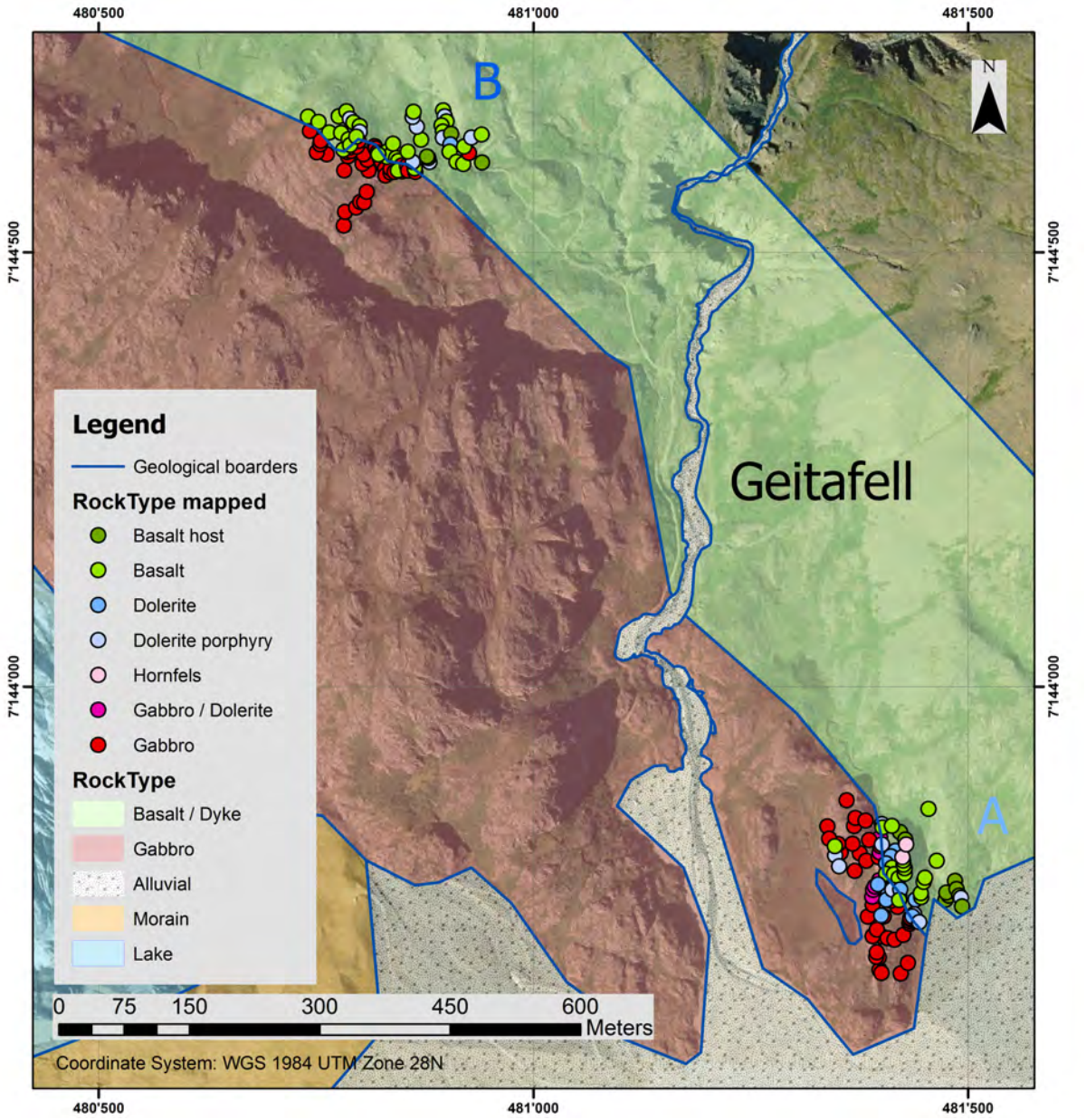

Figure 8: Geological mapping was done at two locations (A and B) where there was considered to do geophysical field measurements later on. Many outcrops were analysed in detail followed by identifying the rock type. Afterwards, a contact line was drawn between gabbro and basalt (host rock). To mention is that this line can be trusted where it was mapped on outcrops but not really everywhere else because sometimes it is rather difficult to find the exact transition. The outer border of basalt / dyke which can be seen in the top right corner is not really a border but no more geological field work was done there. So, it can be assumed that basalt will continue there but with fewer dykes.

2.3 Profile lines

Figure 9 below shows locations of all geophysical profiles in relation to the geology. Three lines are in Geitafell (A, B, C) and three in Hoffell (X, Y, Z). More detailed information about each of them are given below and illustrated in Figures 9 - 14.

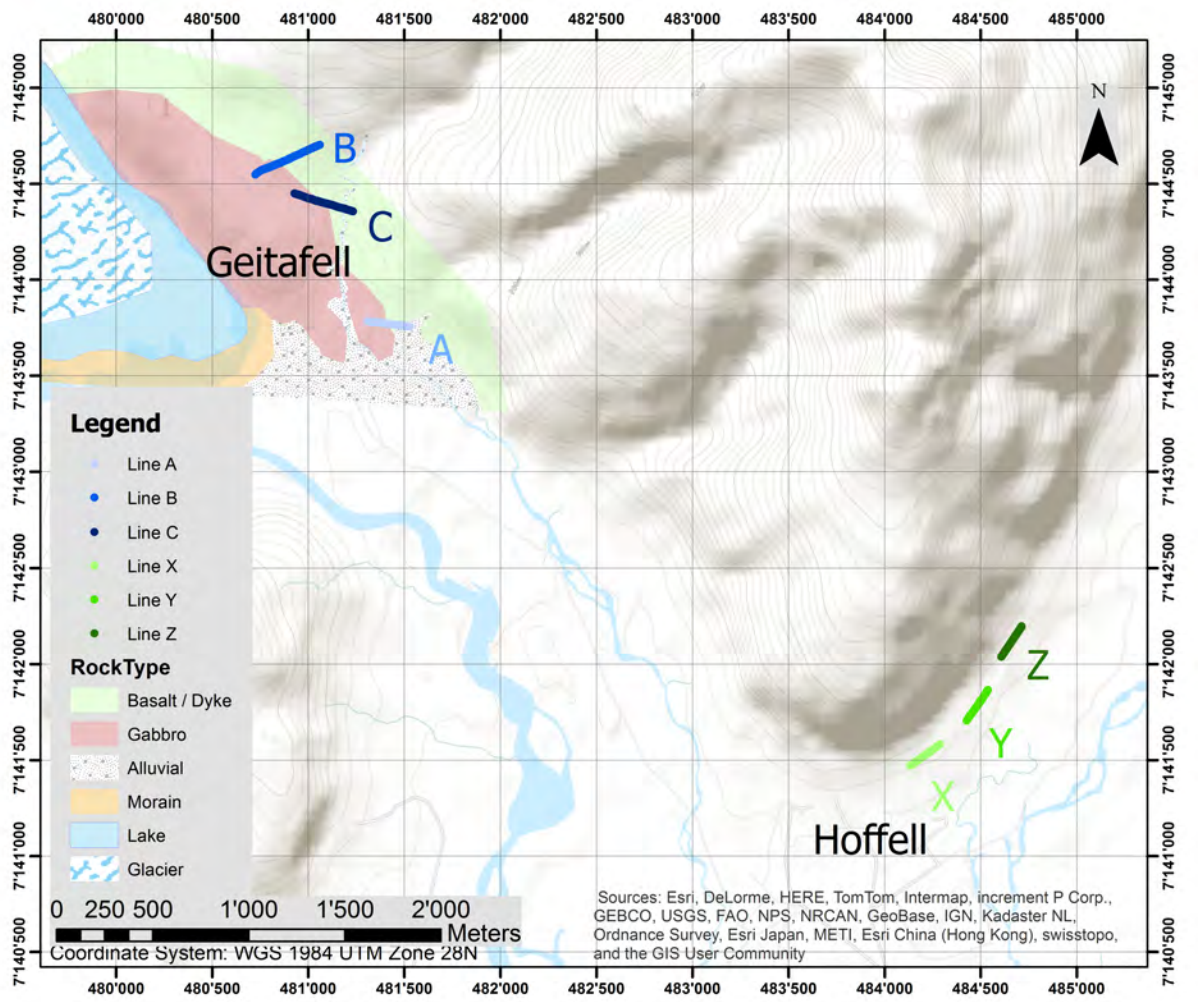

Figure 9: Location map of all profile lines in relation to the geology. Three lines were chosen at Geitafell (A, B, C) and three at Hoffell (X, Y, Z). Line X is in the actinolite zone, line Y is in the garnet zone and line Z is in the epidote zone (see Appendix B, Figure 43).

2.3.1 Geitafell

Figure 10 shows the profiles superimposed on a photograph of the area Geitafell. In the follwoing paragraphs I describe each one individually.

Figure 10: The three geophysical profile lines at Geitafell superimposed on a photograph of the area. All lines start in the host rock (basalt) and end towards the center of the picture in the gabbro.

Line A

The contact zone between the magma intrusion (gabbro) in the west and the surrounding hostrock (tholeiite lava; basalt) in the east is shown in Figure 11. It is intersected with several dykes, cone sheets and acid phases. Hornfels (∼2-5 metres thick) can be found at this boundary due to contact metamorphism. Tholeiite lava has seen several alterations due to the cooling (maximum actinolite). The first few electrodes/geophones in the east of line A were planted in alluvial material (gravel). The topography increases towards the west where small rocky hills appear alternately with flat regions consisting of soggy soil. The soil at the west end of the seismic line is fully saturated with water. Both the seismic line and DC electric line had the same starting point A (first geophone / first electrode) but not the same finishing point A'. We were able to plant in 96 electrodes. This leads to a total profile length of 190 metres using a two metres spacing. This was the maximum length we could reach for the DC electric measurements due to limited electrode cables in the field. More cables were available for the seismic measurements, hence 120 geophones recorded signals during the measurements, giving a total profile length of 238 metres.

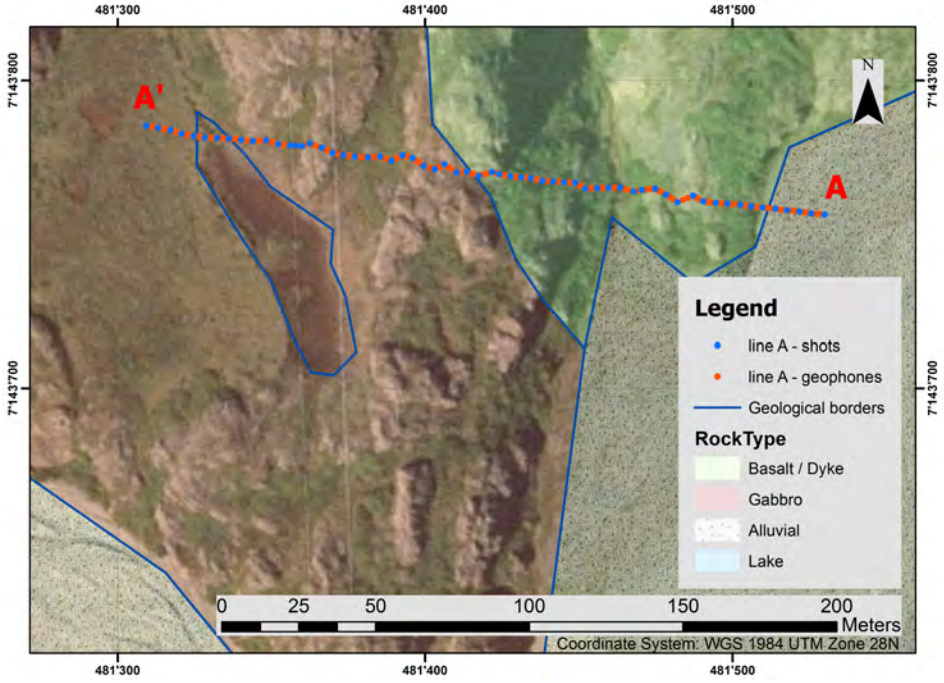

(a) Geophone and shot positions of line A.

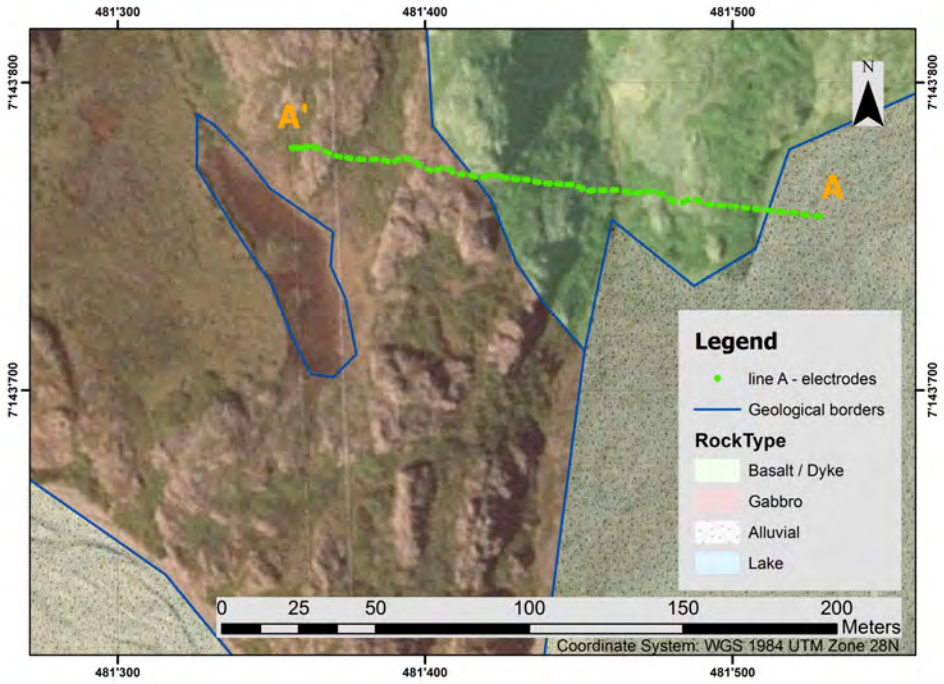

(b) Electrode positions of line A.

Figure 11: Seismic and DC electric measurements at line A in relation to the local geology. Shown are all electrode and geophone positions with each having a 2 m spacing to the next one. 96 electrodes and 120 geophones were used, hence this leads to a total length of 190 m and 238 m, respectively. 61 shots were recorded for the seismics (every 4 m one shot). The starting point A was the same for both seismics and DC electrics.

Line B

This line is the longest seismic line with a total length of 382 metres (192 geophones). It starts in toleiite lava (basaltic rocks in the actinolite zone intersected by several dykes) in the east. This area consists partly of gravel which covers the hard rock. More outcrops can be seen towards the middle of the line where rocky parts alternates with parts of rocks covered by vegetation. The line crosses then the contact zone consisting of hornfels before it ends in the gabbro where the rocks are again well visible. The location was chosen among other things due to the flat topography. There are some steep parts, especially close to the small river in the eastern part of the line and also close to the geological border (gabbro/basalt). But otherwise also due to the small road it is very good accessible. The same positions but less cables were used for the DC electric measurements (total length: 198 metres). The actual positions of geophones, shot locations and electrodes are shown in relation to the local geology in Figure 12.

Line C

Line C is characterised by large altitude differences (∼60 metres). Figure 13 shows all positions where geophones or electrodes were pushed into the ground, again in relation to the local geology. Both measurements started at the same starting point C. There we can find basalt with an increasing amount of dykes intersecting towards the contact zone. A river (north-south) crosses the profile line (east-west) where one can find a lot of unconsolidated material in various sizes. The topography increases on both sides of the river by several tens of metres. The rocks are mostly covered by vegetation. Outcrops of gabbro can be seen towards the end of the line in the west. Some parts were too steep and slippery during the seismic measurements and this is the reason why some shot locations are missing there. Otherwise we recorded the seismic signals using 168 geophones from shots at an interval of four metres. The total distance of the DC electric measurement is again only 190 metres, while the profile length for the seismic measurement is 332 metres.

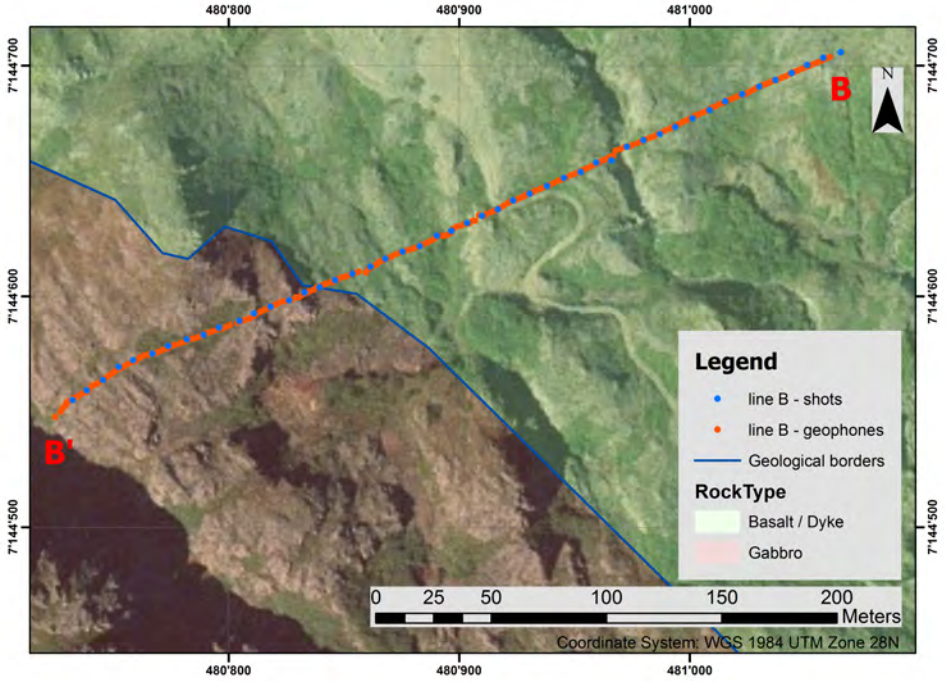

(a) Geophone and shot positions of line B.

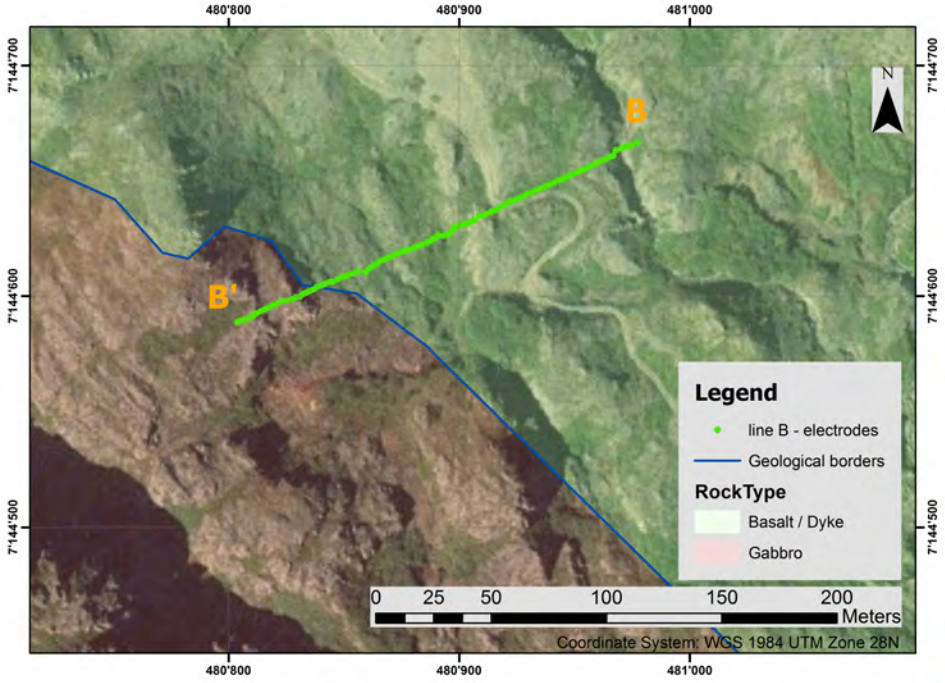

(b) Electrode positions of line B.

Figure 12: Seismic and DC electric measurements at line B in relation to the local geology. Shown are all geophones (192) and shot locations (each 8 m one shot). The total length from the first geophone to the last is 382 m. The distance between two geophones/electrodes is 2 m. 100 electrodes were planted in, leading to a total length of 198 m for the DC electric line.

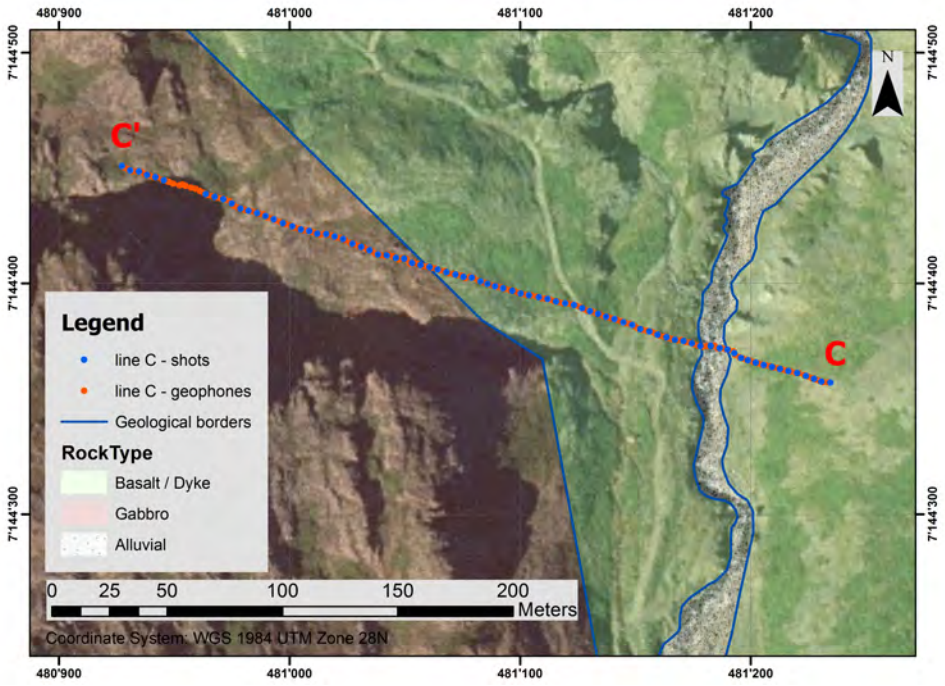

(a) Geophone and shot positions of line C.

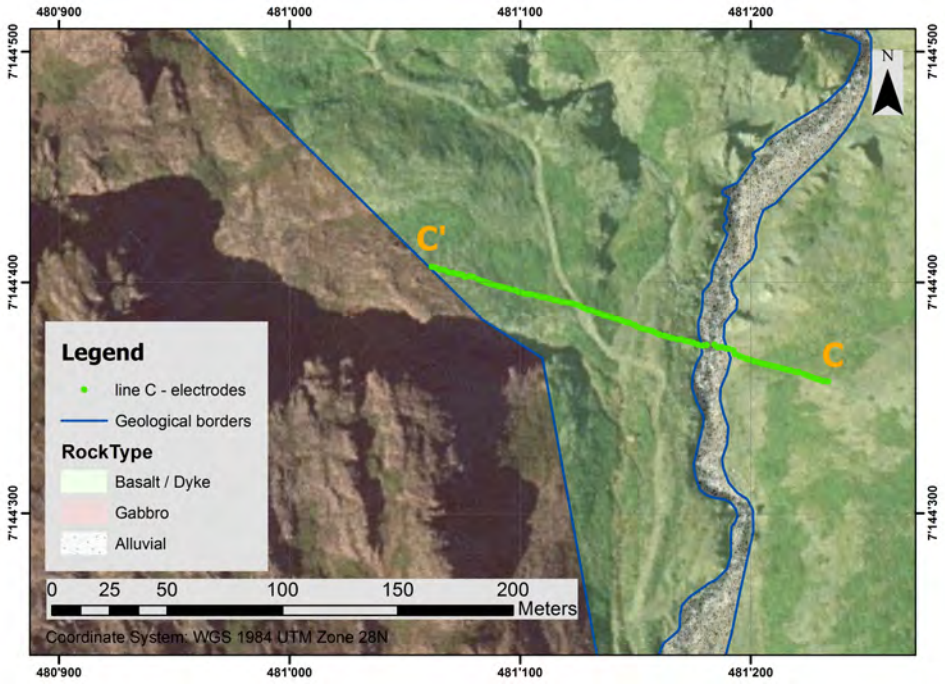

(b) Electrode positions of line C.

Figure 13: Seismic and DC electric measurements at line C in relation to the local geology. In total, 7 cables with each 24 geophones were used (total length along the topography: 332 m). Shots were done every 4 m. Both geophones and electrodes have a 2 m spacing. 96 electrodes were used (total length: 190 m). The starting point C was the same for both measurements.

2.3.2 Hoffell

Three locations in Hoffell were chosen to measure electric and elastic properties of basaltic rocks. They are shown in Figure 14 superimposed on a photograph of the area. The aim was to take measurements at different alteration zones. These appear here on flat soil. Therefore these locations looked to be suitable when considering the map of Omar Fridleifsson (Appendix B, Figure 43) where everywhere else topography plays a much larger role. Line X is in the actinolite zone, line Y is in the garnet zone while measurements on line Z represent the epidote zone. All seismic and DC electric lines have a total length of 190 metres and 198 metres, respectively (two metres spacing of geophones and electrodes). The local geology consists of toleiite lava layers (each ∼3 metres thick) which all have a slightly different appearance. Homogeneous basalt, basalt with vesicles and dolerite with or without porphyric crystals are the main constituents of these layers. Most of the rocks on the outcrops are heavily weathered. Gravel and a soggy soil cover almost everywhere the top lava flow layer. But some parts are visible at the surface due to the fact that these layers are dipping a few degrees.

Figure 14: Locations of the three geophysical profile lines at Hoffell superimposed on a photograph of the area. Line X is in the actinolite zone; Line Y is in the garnet zone; Line Z is in the epidote zone. The lines in the picture are only drawn approximately on their real locations.

3 Methods and Techniques

Two geophysical methods, electrical resistivity tomography (ERT) and seismic refraction tomography (SRT), were chosen to estimate physical ground properties and to image the first few tens of metres of the subsurface. The basic physical principles and some processing steps are outlined below. In addition, seismic velocities of collected rock samples were measured in the Rock Physics lab at ETH Zurich.

3.1 Electrical resistivity tomography

3.1.1 Basic principle of DC electrics

Ohm's Law defines the resistance R by the ratio of the potential drop to the applied current.

$$R = \frac{V}{I} \tag{1}$$

The resistance of a given subsurface body is proportional to the specific length L and inversely proportional to the area A:

$$R = \rho \frac{L}{A} \tag{2}$$

The proportionality constant ρ is the true resistivity and a fundamental point property of each material. Figure 15 explains formulae (1) and (2) by means of a simple sketch.

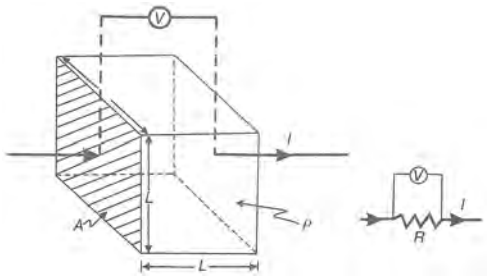

Figure 15: Electrical circuit, where R is a resistor, V is the potential difference across R, and I is the injected current. L is a length and A is a surface on the block [Reynolds, 2011].

Resistivity is determined trough a combination of equation (1) and (2) and is the product of the resistance and a length:

$$\rho = \frac{VA}{IL} [\Omega m] \tag{3}$$

If the ground is not uniform, the obtained resistivities are no longer true resistivities but so called apparent resistivities ρ_a. Apparent resistivity is the product of the measured resistance R and the geometric factor K for a given electrode array:

$$\rho_a = RK[\Omega m] \tag{4}$$

where

$$R = \frac{\Delta V}{I}[\Omega] \tag{5}$$

$$K = 2\pi[\frac{1}{AM} - \frac{1}{MB} - \frac{1}{AN} + \frac{1}{NB}]^{-1}[m] \tag{6}$$

In (6) A and B are the positions of the current electrodes, while M and N are the positions of the potential electrodes.

Numerous array types exist but two of the more common ones, Wenner and Dipole-Dipole, are depicted in Figures 16 and 17. These types of electrode configurations have different current flow patterns and therefore different sensitivities, see Figure 18 and 19. The sensitivities depend on the electrode configuration as well as the subsurface model.

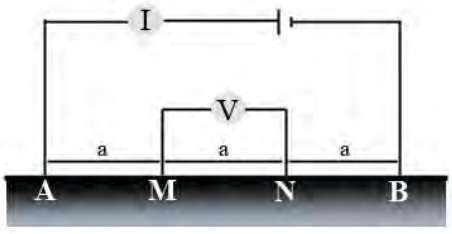

Figure 16: Wenner configuration. A and B are current electrodes while M and N are potential electrodes. $\rho_a = 2\pi aR$. Sketch based on [Lowrie, 2007].

Figure 17: Dipole-Dipole configuration. A and B are the current electrodes while M and N are potential electrodes. $\rho_a = \pi n(n+1)(n+2)aR$. Sketch based on [Lowrie, 2007].

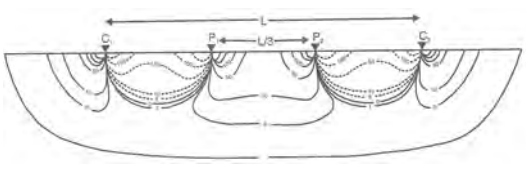

Figure 18: An example of the subsurface sensitivity from a Wenner configuration is shown in this figure. This type of configuration has a good vertical resolution [Reynolds, 2011].

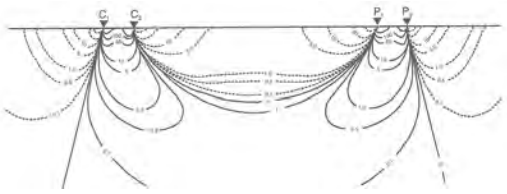

Figure 19: An example of the subsurface sensitivity from a Dipole-Dipole configuration is shown in this figure. This type of configuration has a good lateral resolution [Reynolds, 2011].

3.1.2 Data acquisition

The targeted depth at Geitafell was about 20 to 30 metres in order to avoid measuring only weathered rocks. In addition, a vertical and horizontal resolution of a few metres was needed to delineate the contact zone. Therefore, an electrode spacing of two metres was selected for all geophysical profiles to fulfil these two criteria.
A multi-electrode resistivity system (Syscal or Geotom) was used, which can measure several configurations at the same time. Ninety-six electrodes can be connected to the system Syscal, while the Geotom has 100 channels available. This gives a total horizontal length of 190 and 198 metres along the topography. The device Syscal was favored for field measurements due to its stronger currents (hence power), which can be injected into the subsurface. But the backup device Geotom had to be used in the field on several occasions due to technical problems with the Syscal. Table 1 stipulates which system was used on each profile.
Three different types of electrode configurations (Wenner, Dipole-Dipole and Schlumberger) were used to achieve a combined good coverage and optimal resolution of the subsurface [Reynolds, 2011]. Numerous depth levels (increasing distance a in Figure 16) were tested in the field but 16 levels was decided to use most of the time. Each injected current pulse was repeated four (minimum) to ten (maximum) times. These measurements were stacked until the standard deviation was smaller than a certain value (dependent on field conditions between 3-10 % of the measured voltage) or reached the maximum number of stacks. These values indicate the repeatability, the smaller the better. A complete set of measurements for one electrode geometry such as Wenner array involves between 1'000-2'500 measurements until all depth levels are covered.
Igneous rocks tend to have high resistivities, but resistivity also depends on the mineralogy (secondary minerals) and on the pores and cracks and any fluid which might fill them [Reynolds, 2011, Kirsch, 2009]. Hence the near surface can be very conductive depending on weather conditions.
Potential differences V (voltages), in the range of millivolts, are the values which are actually measured in the field. This measured voltage was then divided by the injected current I (which is in the range of milliamperes and changes for each measurement). The ratio V/I was then multiplied by the geometric factor, which also changes for each measurement, to get the apparent resistivity. Problems arose while measuring the potentials whenever there was poor contact between an electrode and the ground. This can be

mitigated to some extent by pouring salty water around the electrodes and/or planting the electrodes even further into the ground. But such effort is limited and so the surface conditions together with background noise dictate the data quality. At Geitafell there was minimal cultural noise but it was very difficult to drive the electrodes into the outcropping rock.
To summarise, DC electric measurements were carried out with different devices at six locations during the field campaign in Iceland in September 2013. All relevant information can be found in Table 1. A lot difficulties such as poor ground contact, instrument malfunction and changing weather conditions accompanied our measurements.

3.1.3 Data analysis

A computer program called DC2dInvRes was used for qualitative data analysis and for editing the raw data. Pre-processing is best done when the data are assembled in pseudo-section form. Figure 20 shows a pseudo-section of a Wenner measurement from line C. It shows the raw data from the field measurement, where each cell represents one apparent resistivity data point (in Ωm). The horizontal position of the cell is the midpoint between the outer electrodes. The pseudo-depth is related to the electrode separation (equal to $'a'$ in case of the Wenner array or the intersection of the 45° lines from the current and potential dipoles in the case of the Dipole-Dipole array). The larger the pseudo-depth the larger the electrode offset, meaning that the currents penetrated deeper into the ground and therefore the data point represent a deeper zone in the subsurface. Single data points or even all measured data from a single electrode can be easily deleted in this pseudo-section if it appears that it is particularly noisy or spurious.
The data quality can suffer from poor ground coupling and it can also be affected by the geomorphology or other environmental influences. Data points with extremely high resistivity values were deleted as well as data points with a high estimated error. Also some data points were deleted at deeper depth levels where there was little convidence in the 2D nature of the data. I.e. due to 3D effects where current flows probably choose to take a less resistant path around a hill or along the conductive surface instead of flowing deep into the subsurface (line A).
Data quality varies a lot on the different profile lines. A good and a poor example of an edited data set are shown in Figure 20 and 21, respectively.

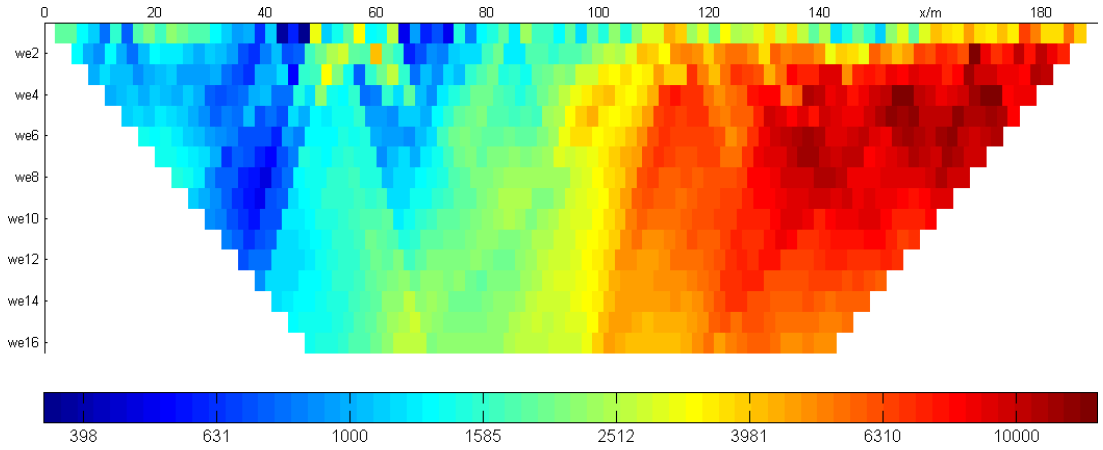

Figure 20: Pseudo-section from line C. The horizontal axis describes the horizontal distance while the vertical axis represents the pseudo depth. The values are in Ωm where low values stand for low resistivity (high conductivity) and high values for high resistivity (low conductivity). This pseudo-section represents a good quality data set.

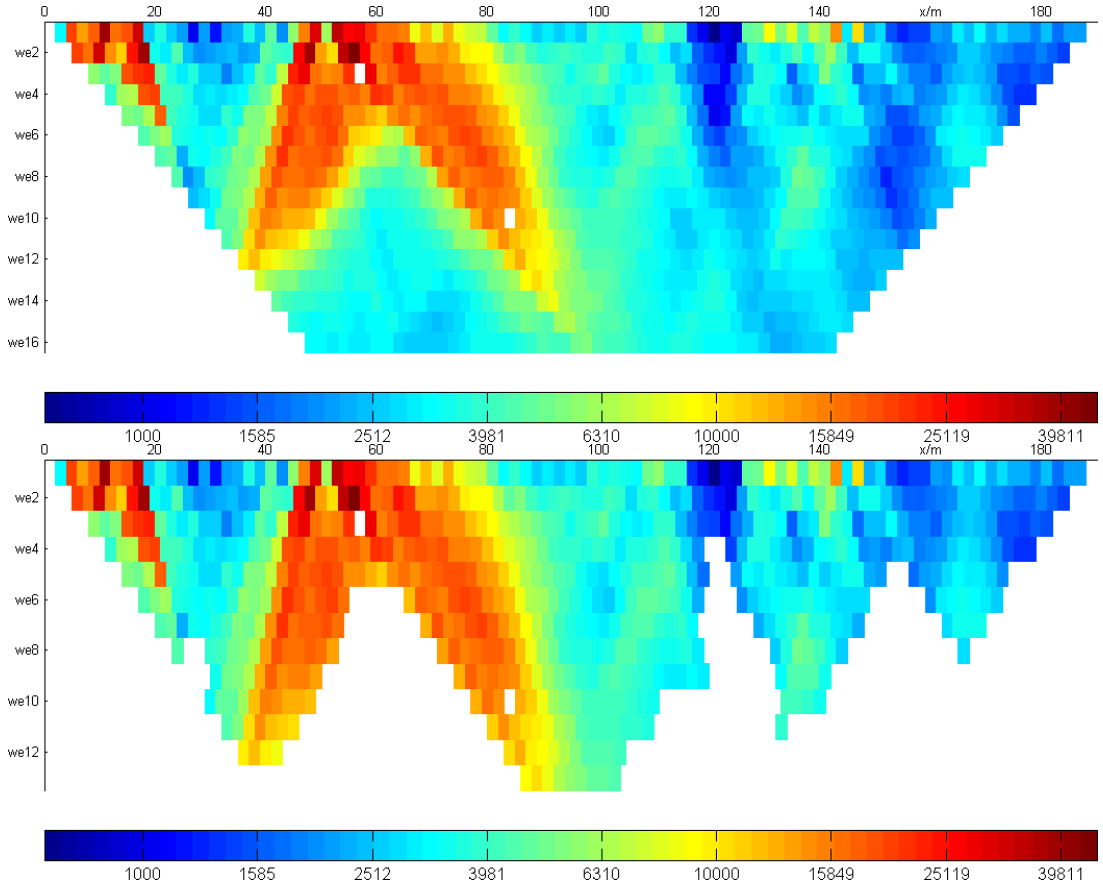

Figure 21: Pseudo-section from line A before and after editing. It represents a poor quality data set in which several data points needed to be deleted.

3.1.4 Data inversion

Synthetic resistivity data, calculated for a specified resistivity model, can be generated and compared with the observed resistivity data by means of the program BERT (boundless electrical resistivity tomography). The inversion progressively adjusts the model to achieve the best fit between the computed (synthetic) and observed (measured) data. The difference between them is measured by the root mean square (RMS) error. Figure 22 shows the main sequences in this inversion.

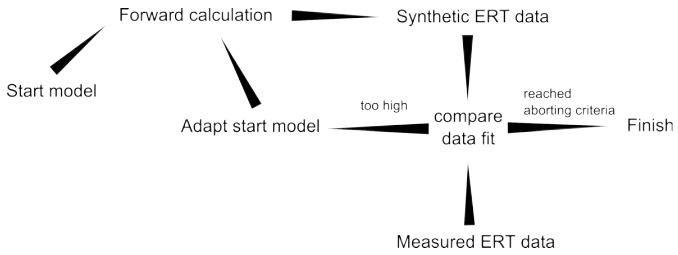

Figure 22: Scheme of a BERT inversion based on the BERT-tutorial [Günther and Rücker, 2013].

A starting or initial guess model (e.g. the pseudo-section) together with all topography information and grid structure information are necessary inputs. The program uses a triangulated grid for both forward modeling and for the inversions. Grid elements get lager towards the side and bottom boundaries. The inversion will be under-determined. This means that there are more equations to solve than data points are available from the measurement. There is not enough information to determine a unique model, several possible solutions exist. Hence constraints need to be added such as smoothing and damping to find a best fit solution of the inverse problem [Günther and Rücker, 2013]. It was decided to apply relatively high smoothing to all profile lines and not necessarily the smoothing factor ending up with the smallest error. Of course the smoothing factor was chosen in the region with the smallest error but other factors were more important. Due the fact that the data quality is moderate and we were not really interested in small untrustworthy features in the model, this high smoothing was applied which leads to much larger structures. The sensitivity pattern in a model indicate at which depth the model can be trusted or not anymore. Low sensitivity areas can change their value in the model but have no effect on the data. So these areas should not be included in the models. They sometimes appeared already at little depths which led to decrease the model depth. All relevant information on the inversion parametres can be found in Table 1.

Table 1: Acquisition and inversion parametres for the DC electric measurements.

	A	**B**	**C**	**X**	**Y**	**Z**
Device	Syscal	Geotom	Syscal	Geotom	Geotom	Geotom
Measured electrode geometry	Dipole-Dipole Wenner Schlumberger	Dipole-Dipole Wenner	Dipole-Dipole Wenner Schlumberger	Dipole-Dipole Wenner	Dipole-Dipole Wenner	Dipole-Dipole Wenner
# Electrodes	96	100	96	100	100	100
Electrode spacing	2 m	2 m	2 m	2 m	2 m	2 m
Profile length	190 m	198 m	190 m	198 m	198 m	198 m
Used geometry for final model	Schlumberger	Wenner	Wenner	combined wen/dip-dip	combined wen/dip-dip	combined wen/dip-dip
Smoothing λ	200	200	200	20	30	20
Model depth	10 m	10 m	30 m	7 m	10 m	10 m
RMS error	18.4%	26.6%	20.1%	19.4%	12.0%	12.0%

3.2 Seismic refraction tomography

3.2.1 Basic principles of refraction seismics

Seismic waves propagate through the subsurface along various paths but the first arrivals follow the high velocity parts of the subsurface. At a velocity contrast, the waves will change direction in accordance with Snell's law:

$$\sin i / \sin r = V_1/V_2 \tag{7}$$

$$\sin i_c = V_1/V_2 \tag{8}$$

where (7) is the formula for general refraction and (8) is the formula for critical refraction. They are shown in Figure 23. Quantifies i and r are the angles of incidence and refraction, while i_c is the angle at which critical refraction occurs i.e. r=90°. Critical refraction only occurs if velocity increases with depth, that is if $V_2 > V_1$. If there is a gradual change in velocity with depth, the rays are curved. This means that the wave is continuously refracted (diving wave).

A seismic source (e.g. hammer or shotgun) generates a seismic wave which propagates through the subsurface along various paths (eg. direct, reflected, refracted, critically refracted or diving waves) and are then detected by geophones at certain offset distances along the ground surface (see Figure 23). The first arrivals will then be used to calculate a subsurface velocity model [Reynolds, 2011]. The velocities are dependent on rock composition, density, temperature, pressure, the presence of fluids and the degree of fracturization [Huenges and Ledru, 2010].

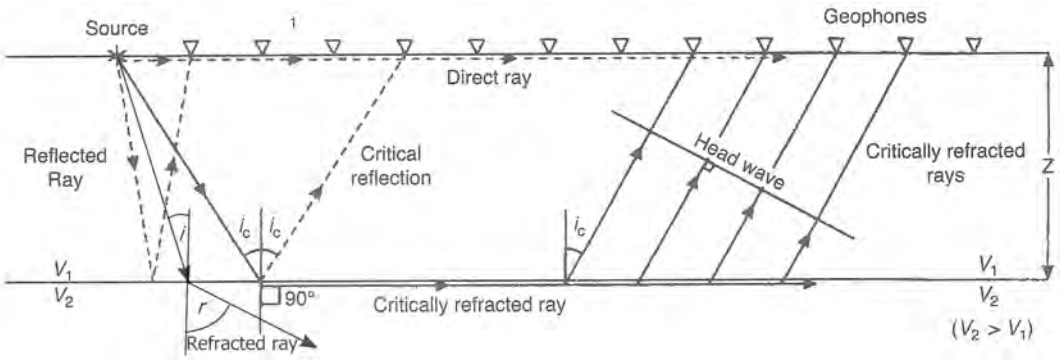

Figure 23: Raypath diagram, showing paths for direct, reflected, refracted and critically refracted rays [Reynolds, 2011].

3.2.2 Data acquisition

Seismic measurements were taken at all six locations in Geitafell. The focus was on the same target depths and resolutions as for the DC electric measurements. The longer the horizontal offset the deeper the ray paths go through the subsurface but the greater the offset, the weaker the signal. To maximize this but still retain sufficient resolution, a 2 metre spacing between geophones was employed. Different numbers of cables (each having 24 channels) were used in the field at the various sites depending on access and predefined targets. A maximum of eight cables was laid out at line B, hence a maximum horizontal offset of nearly 400 metres was reached on this line. The length of each line and the number of recording channels are listed in Table 2.
The source was normally a shotgun (blank cartridges, bore 12) which was buried around half a metre into the ground. This went well at places where small holes could be drilled into the surficial soil. Everywhere else where hard rock was at the surface and it was impossible to use the shotgun, a hammer (4.5 kg) was used for the seismic source. This weaker hammer source was stacked ten times to yield a similar source intensity to the shotgun. The distance between each shot was four metres with a few exceptions. All relevant information on the seismic acquisition is summarised in Table 2.

3.2.3 Data analysis

A qualitative data analysis was done by looking at the raw data in shot gather as well as receiver gather format. This gave a first impression of the quality of the data, hence noisy traces could be identified. Poorly coupled geophones, dead traces and misfires were deleted from the data. The shot gather also showed how far away the first breaks could be seen clearly and at which distance the noise mastered the seismic signal and no clear first break could be seen anymore. Some of the shots gave clear first breaks on all geophones and could be reliably picked. Others are almost everywhere overprinted by noise. Figure 24 shows a good and a poor example of a shot gather. Each line had different weather and ground conditions, hence data quality differs a lot between the lines but also between the shots. Unfortunately, almost all data contained a lot of noise, hence the quality was rather poor in general. The cause was mainly strong wind and rain but also the sometimes unstable contact between geophones and the ground.
The geometry information was added to the raw data and first arrivals were then picked using a Matlab program interface. The picking was done with an accuracy of about one

millisecond. A weighting of picked travel times in the noisy part was considered but in the end travel times were either picked in this noisy part of the gather or were not picked at all. Poor quality data could be assigned a weighting but this did not really make sense because then almost all travel times would get a reduced weighting. So it was just simpler to apply a weighting factor of zero or one to the picked travel times.

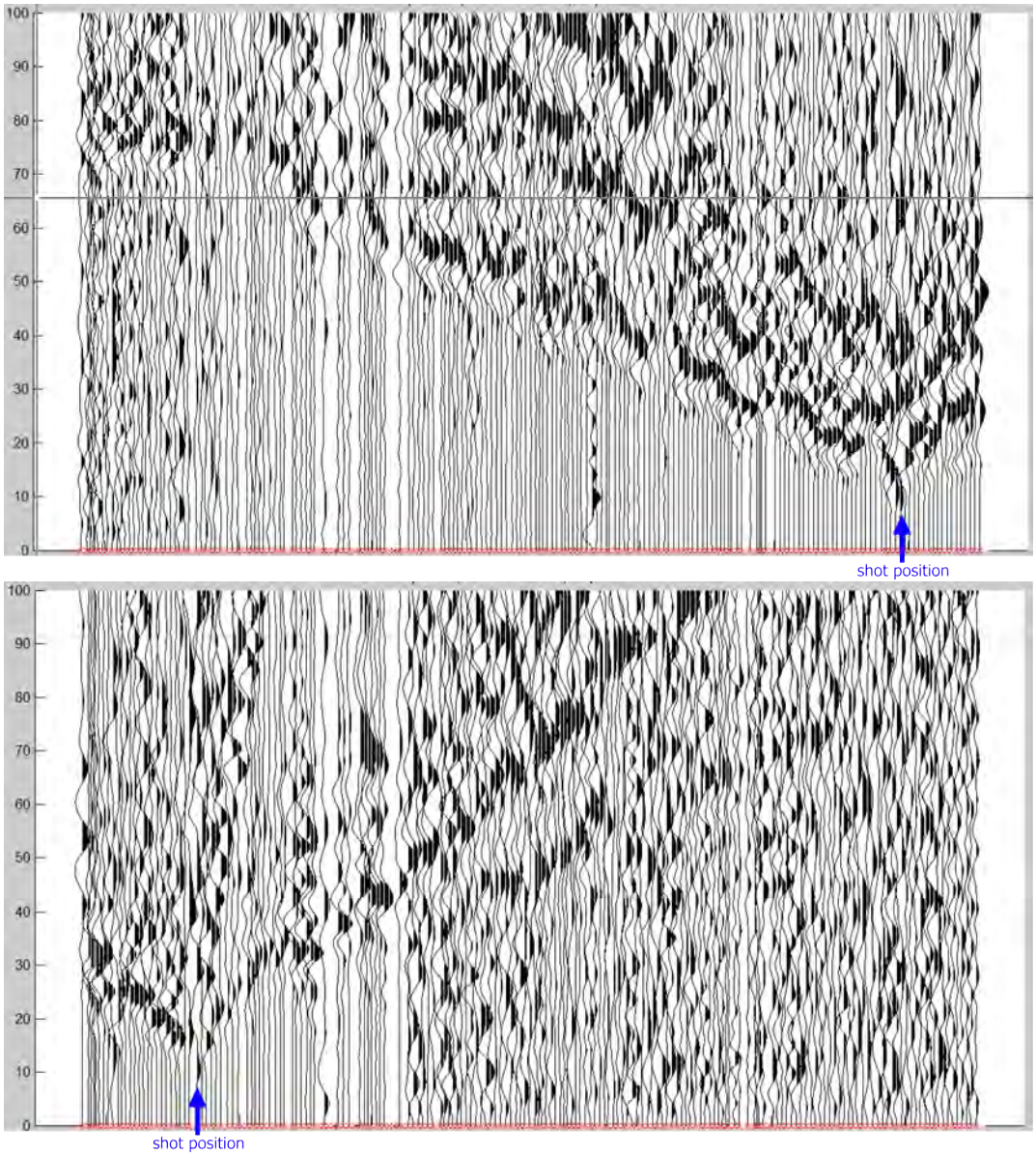

Figure 24: Two shot gathers from line B showing the variation of data quality. The top gather represents a good shot without a lot of noise while the second one contains a lot of noise and the each 2 m apart first breaks are difficult to identify. Each trace (x-axis) corresponds to a different geophone (channel). The vertical (y) axis is the travel time in ms.

3.2.4 Data inversion

The first arrival data set constitute the input to a surface 2-D tomographic algorithm. It uses a fast finite-difference eikonal solver to calculate the predicted times for a given model. The inversion incorporates appropriate damping and smoothing constraints and was developed by Lanz et al. [1998]. Velocity parametres, source-receiver coordinates and an initial model need to be supplied before the synthetic travel times can be computed. The difference between observed and predicted travel times (residuals) are minimized by the inversion. The resultant velocity models can then be tested for reliability by means of ray diagrams or plots of synthetic and observed travel times.

The use of a realistic starting model is very important for all further steps in the inversion. It will make sure that the model updates in the correct direction. Hence several calculations were done but in addition different starting models were tested. Since the program is based on continuously refracted diving waves, which return to the surface, it is essential that the starting model incorporates a positive velocity gradient, i.e. increase of velocity with depth. The aim of this testing was to reach a small error after the first iteration of the observed and the synthetic data. The starting model of each line was adjusted individually due to the different surface topography.

The smoothing and damping factors will then regularise (stabilise the inversion) and adjust the model for further iterations. The smoothing factor regulates the neighboring cells in a model such way that they do not differ too much from each other e.g. minimal roughness. The damping factor regulates how much the model can be adjusted after each iteration and seeks to make it close to the starting model or some preferred model. A high damping factor adjusts the model slowly, hence more iterations are necessary. Several combinations were tested but in the end relative high smoothing and damping factors were chosen for all lines due to the rather poor data quality in order to avoid introducing too small features in the model which cannot be trusted. The other cause was to prevent all rays from taking the same path because the aim was to cover (interrogate) most of the model parts by the rays. All relevant inversion parametres for all lines are given in Table 2.

Synthetic data after the final iteration of the inversion and observed data should overlap each other and show minimal scatter in an offset-time diagram. The agreement or overlap was in some cases well achieved but not everywhere. The spreading of the data in this diagram should also be tightly clustered in a way that all data points are concentrated in

a narrow zone. A good and a poor example of such misfit plots are given in Figure 25. Only area with a good enough ray coverage in the velocity model have high reliability. Therefore cell size was kept the same with depth (relatively small, one by one metre) and a high smoothing was applied. The ray coverage could be improved by these two factors but it was far from optimal. The rays were concentrated in some parts of the model more than others. This was probably caused by the fact that not all shots triggered at the same time. Hence the origin time (onset) differs from shot to shot by several milliseconds and therefore it needs to be corrected. This is referred to as shot static. The idea was to use the already inverted smooth velocity model as the starting model and do the inversion again with only a few iterations, but this time to invert for the origin times as well. This additional feature of the inversion was developed by Maurer [1996]. How much this correction is applied can again be controlled by a damping factor.

To summarise, the whole data inversion was done in two parts. The aim of the first part was to get a smooth velocity model having already a small error between observed and synthetic data. This was then used for the second part in which it was used as the starting model. Only a few iterations were carried out in this part and additionally the origin times were determined, to compensate for the shot static. Parametres can be found in Table 2 and all results together with the ray coverages are shown in chapter 4.

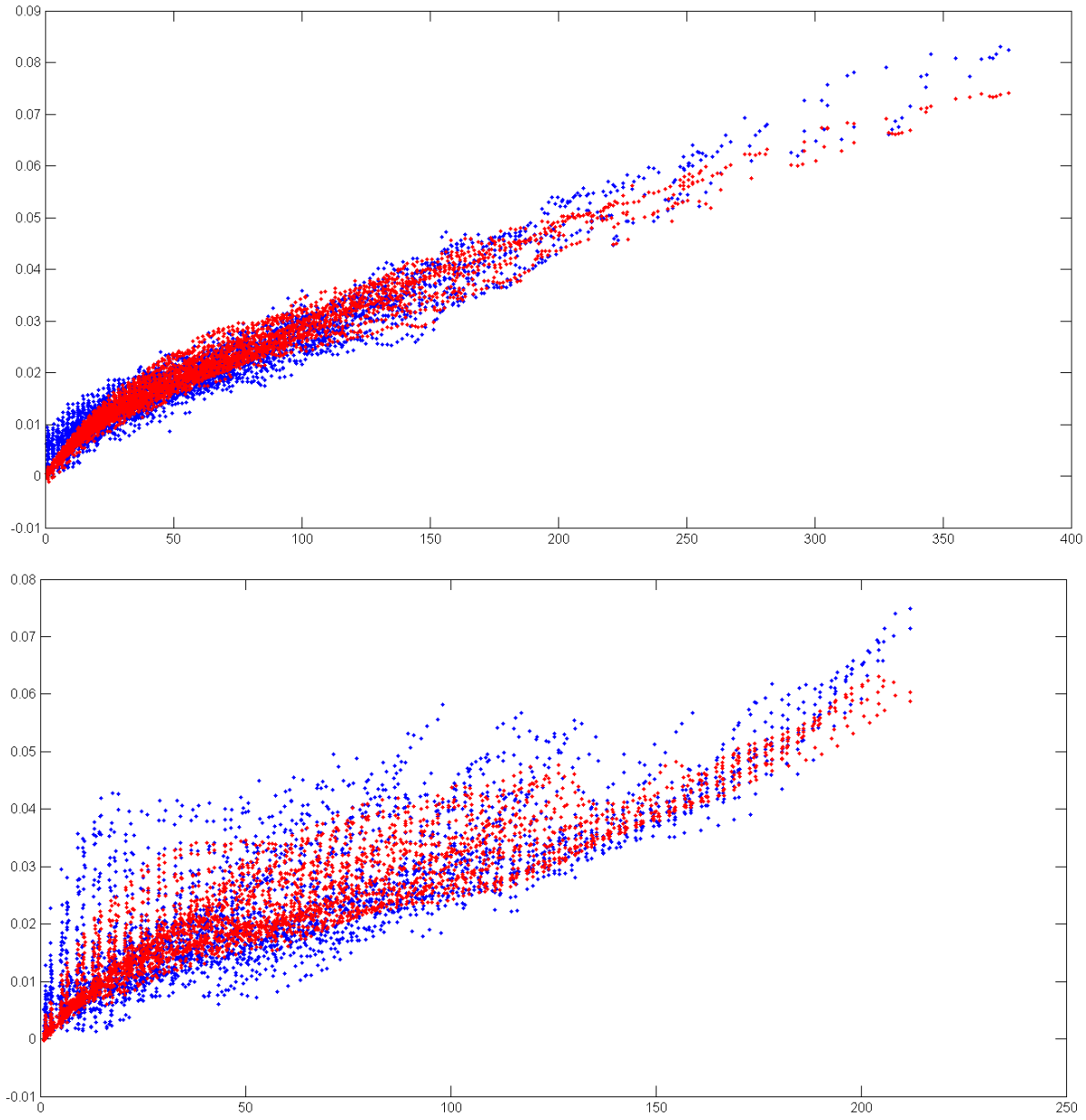

Figure 25: Observed and synthetic data plotted in an offset-time diagram. The blue points are the observed data while the red points represent the synthetic data points after final inversion. The first diagram (line B) shows a good example in which all observed data points are concentrated in a certain zone and the synthetic data points can match them quite good. The opposite can be seen in the second diagram (line A) for a poor quality result.

Table 2: Acquisition and inversion parametres for the seismic measurements.

	A	B	C	X	Y	Z
Geophone spacing	2 m	2 m	2 m	2 m	2 m	2 m
# Channels	120	192	168	96	96	96
Profile length	238 m	382 m	332 m	190 m	190 m	190 m
Source spacing	4 m	8 m	4 m	4 m	4 m	4 m
# Shots	61	48	82	53	49	49
Source type	shotgun 10 x hammer	shotgun 4 x hammer	shotgun 3 x hammer	shotgun	shotgun	shotgun
Geophone type	30 Hz	30 Hz	30 Hz	30 Hz	30 Hz	30 Hz
Sampling inverval	0.0625 ms	0.125 ms	0.125 ms	0.125 ms	0.125 ms	0.125 ms
Record length	1 s	1 s	1 s	1 s	1 s	1 s
Special weather conditions	—	windy	rainy	windy	windy	windy
Depth of model	60 m	60 m	90 m	40 m	40 m	40 m
Smoothing / Damping factors	80 / 80	80 / 80	80 / 80	80 / 80	80 / 80	80 / 80
RMS error	2.5 ms	1.9 ms	2.1 ms	1.8 ms	2.0 ms	1.4 ms

3.3 Seismic velocity analysis in the lab

Vp and Vs measurements were carried out on the collected rock samples from the field site in the Rock Physics lab at ETH Zurich. An ultrasonic pulse (1 MHz) was fed to a source transducer (transmitter Tx) on one side of the sample and the arrival times were then measured on the opposite side by means of another piezoelectric transducer (receiver Rx). To get velocities from these arrival times, the sample length needs to be known as well. The densities and porosities of the samples were also determined for completeness. The first arrival times were picked under several pressure conditions (10 - 250 MPa) due to the expected increase in velocity with continuous increasing pressure (closure of cracks). Data quality was much better compared to the data quality from the field measurements. An example of the first break picking together with a scheme of the laboratory device is shown in Figure 26. Note that the lab velocities are usually higher than field velocities due to the use of much higher frequencies in the lab, and also the lab samples are usually in-fact specimens unlike the field situation where cracking and fracturing may occur.

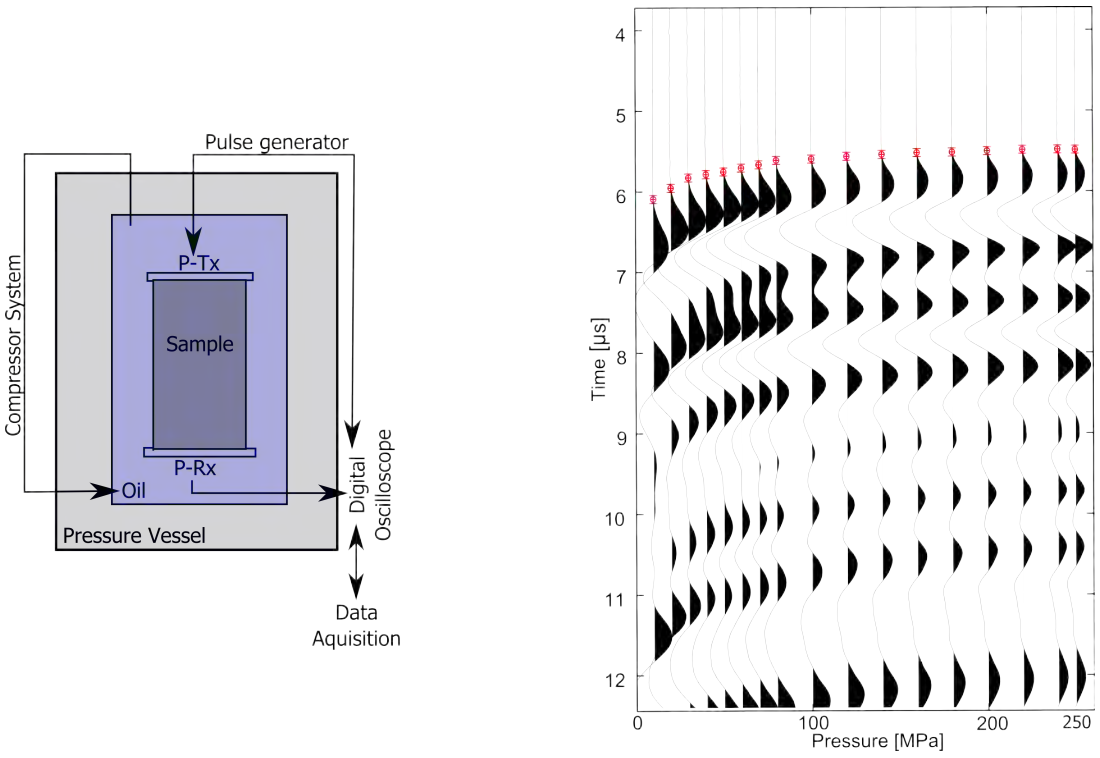

Figure 26: Scheme of the laboratory device (modified after [Shih, 2012]) and diagram with first break picking from arrival times (P-waves) under different pressure conditions (10-250 MPa). The data shown here are from a rock sample which was collected from line Y from the geophysical measurements.

A part of this study is to find out more about the relation between seismic field measurements and seismic lab measurements. Only P-wave velocities were measured in the field and therefore my focus here is also on the P-waves in the lab under dry conditions. The collected rock samples can be categorised from several point of views. Four different aspects are described below, in which the first two are more important for this study:
Firstly, we were interested in the seismic velocities of the following rocks: gabbro, dolerite, hornfels and basalt. This is the same sequence as it was found in the measured geophysical field profiles A, B and C. It starts in the old magma chamber (gabbro) with a lot of dyke material (dolerite). Hornfels can be found at the transition to the altered host rock (basalt). Figure 27 shows photographs of these four rock samples.

(a) Gabbro (b) Dolerite (c) Hornfels (d) Basalt

Figure 27: Rock samples from each lithological unit found on the profile lines A, B and C. Starting from the old magma chamber towards the altered host rock.

Secondly, we were interested in the elastic properties of different host rock material. Each experienced a different degree of alteration. The first rock sample was selected from the actinolite zone, while the second one is from the garnet zone and the third one was collected from the epidote zone (see photographs of samples in Figure 28).

(a) Basalt actinolite zone (b) Basalt garnet zone (c) Basalt epidote zone

Figure 28: Rock samples (basalt) from different alteration zones. To notice is that the rock sample from the epidote zone additionally has vesicles.

The host rock (basalt) tends to include a variable amount of vesicles. Some have no inclusions, others have small ones and some are filled. Their composition can vary a lot but they consist of typical secondary minerals such as actinolite, epidote, chlorite, zeolite, quartz, calcite, garnet or pyrite. Some can also be filled with gas/air. To see how the elastic properties change with the amount of vesicles present, the rock samples shown in Figure 29 were also measured in the Rock Physics lab.

(a) Basalt with no vesicles.

(b) Basalt with a few vesicles.

(c) Basalt with vesicles.

(d) Basalt filled with vesicles.

Figure 29: Rock samples (basalt) with differing numbers of vesicles present.

Not only the basalt varies in its constitution but also the dolerites. Some have a similar grain size (aphyric) others tend to be porphyric. Three examples of dolerites are shown in Figure 30.

(a) Dolerite aphyric 1

(b) Dolerite aphyric 2

(c) Dolerite porphyric

Figure 30: Different types of dolerites (aphyric and porphyric).

4 Results

4.1 Subsurface models at Geitafell (Profiles A, B and C)

The velocity and resistivity subsurface models derived for line A are shown in Figure 32. The velocity model should be viewed with caution and is less important for the final analysis due to a rather poor ray coverage (rays are highly concentrated on certain paths). The resistivity model is equally problematic, it yields little more information about the surface conditions than a differentiation of rock types. The soggy soil parts as well as the subsurface consisting of gravel and the parts which are covered by vegetation represent the conductive (<2'000 Ωm) area in the subsurface model. The high resistive area (>8'000 Ωm) represents a hard rock surface where it was difficult to plant the electrodes. So both subsurface models are not used for further interpretations, unlike subsurface models from line B and C.

Subsurface models (velocity and resistivity) from line B and C are shown in Figure 33 and Figure 34, respectively. Their quality is moderate (ray coverage and ray distribution) and interpretations are reasonable to make. The velocity models show a trend of increasing velocity towards the west. The subsurface velocity models can also be split into three sections. The first five metres are unconsolidated and weathered rocks (<2'000 m/s). The next ten metres (up to a velocity of about 4'500 m/s) are rocks which are probably affected by surface nearby fractures. The third section (>4'500 m/s), starting at around fifteen metres below the surface, is fresh material. Hence this is the depth used for the analysis. Typical velocities for basalt (intersected with dykes and sheets) are extracted (see Table 3) from the models close to an area where they were localised trough the well drilling. Velocity values for gabbro are extracted (see Table 3) from an area where we know gabbro to appear outcrop. Indications can be found at the surface from geological mapping and it is assumed that the rock type will not change with depth at this location. To summarise, typical values were chosen from a certain depth, where no more weathered rock is expected and the ray coverage is adequate. Further information such as the borehole information and geological mapping was taken into account. An example from line B is shown in Figure 31.

The extracted resistivity values at site B and C represent also mainly the surface conditions (Figure 33 and 34) but unlike site A, a trend of increasing resistivity towards the west can be seen in the resistivity subsurface models. The most reliable resistivity sub-

surface model (in terms of geological interpretation) is by far the one from line C. A few metres of weathered rocks can be identified close to the surface (btw. these weathered partly unconsolidated rocks is indicated in all seismic profiles by velocities which are less than 2'000 m/s). The area where gabbro can be expected has resistivity values around 10'000 Ωm while the area with basalt (intersected with dykes and sheets) show resistivity values between 2'000-5'000 Ωm. All these values refer to the fresh material. No values from weathered rocks or unconsolidated and saturated material were included.
Weathered rocks close to the surface can be identified both from velocity and resistivity models. But no clear contact zone between the old magma chamber (gabbro) and the surrounding host rock (basaltic lava flows intersected with sheets and dykes) can be identified. Instead, it is possible to extract certain typical values from the subsurface models and they are listed in Table 3.

Table 3: Typical values (P-wave velocities and resistivities) extracted from the subsurface models at Geitafell.

Rock type	**P-wave velocities** $[m/s]$	**Resistivities** $[\Omega m]$
Gabbro	5'300 - 6'500	$\sim$ 10'000
Basalt (intersected with sheet and dykes)	4'700 - 5'300	2'000 - 5'000

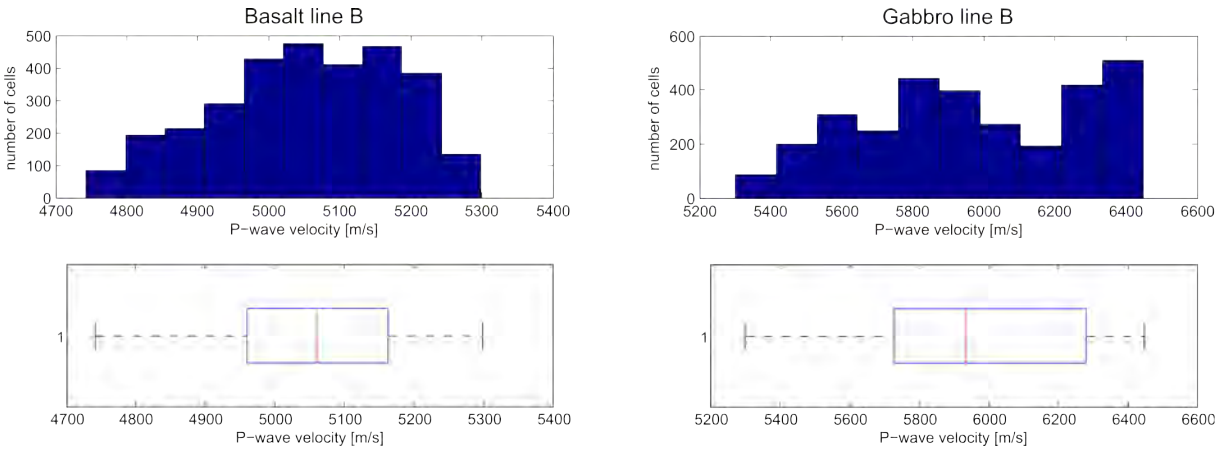

Figure 31: Histogram and boxplot of basalt and gabbro P-wave velocities from line B. The values involved come from the areas of the white boxes marked in Figure 33.

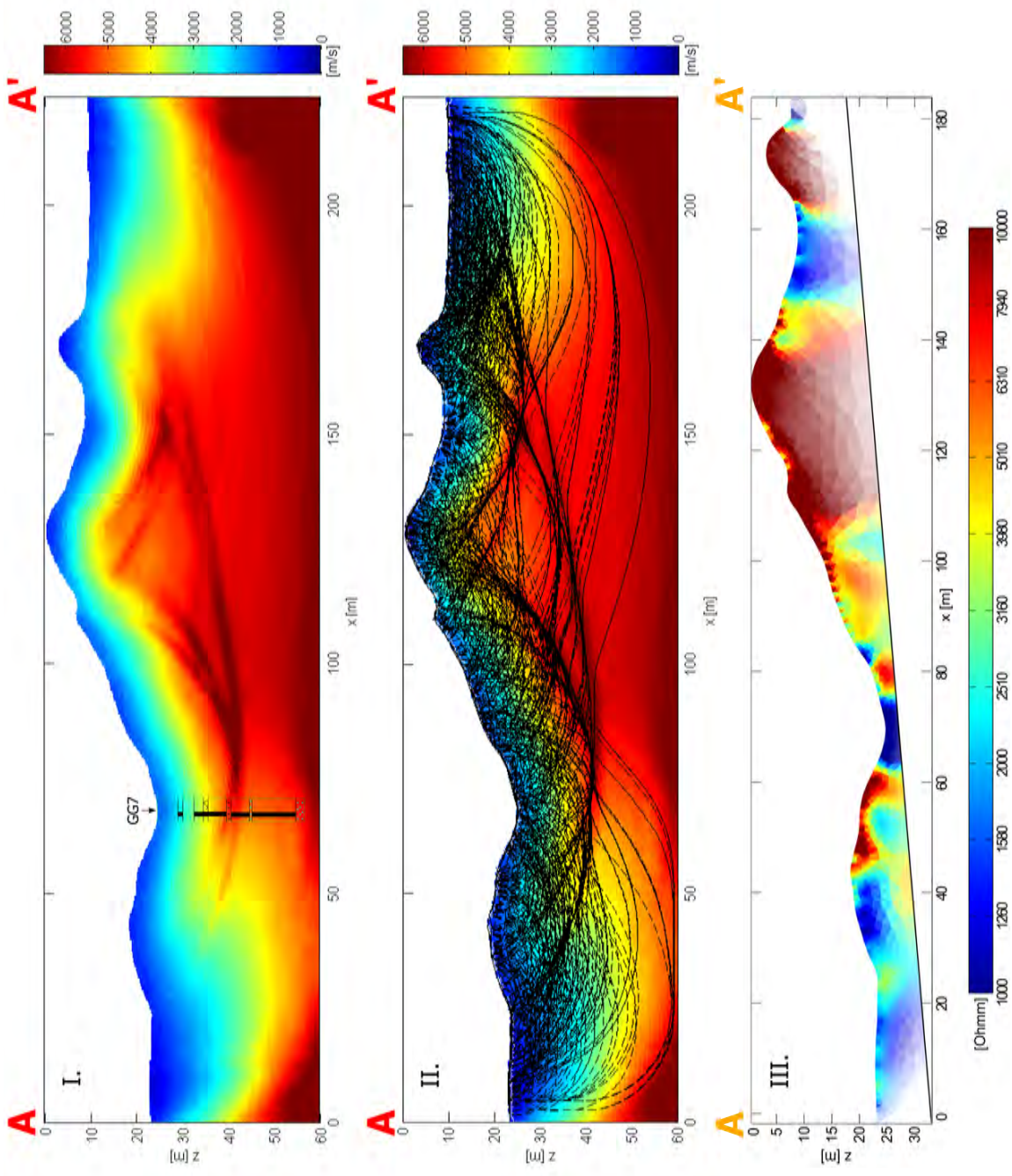

Figure 32: Results from line A. I. shows the P-wave velocity model (RMS error: 2.5 ms). II. shows the ray coverage. III. is the subsurface resistivity model (RMS error: 18.4 %).

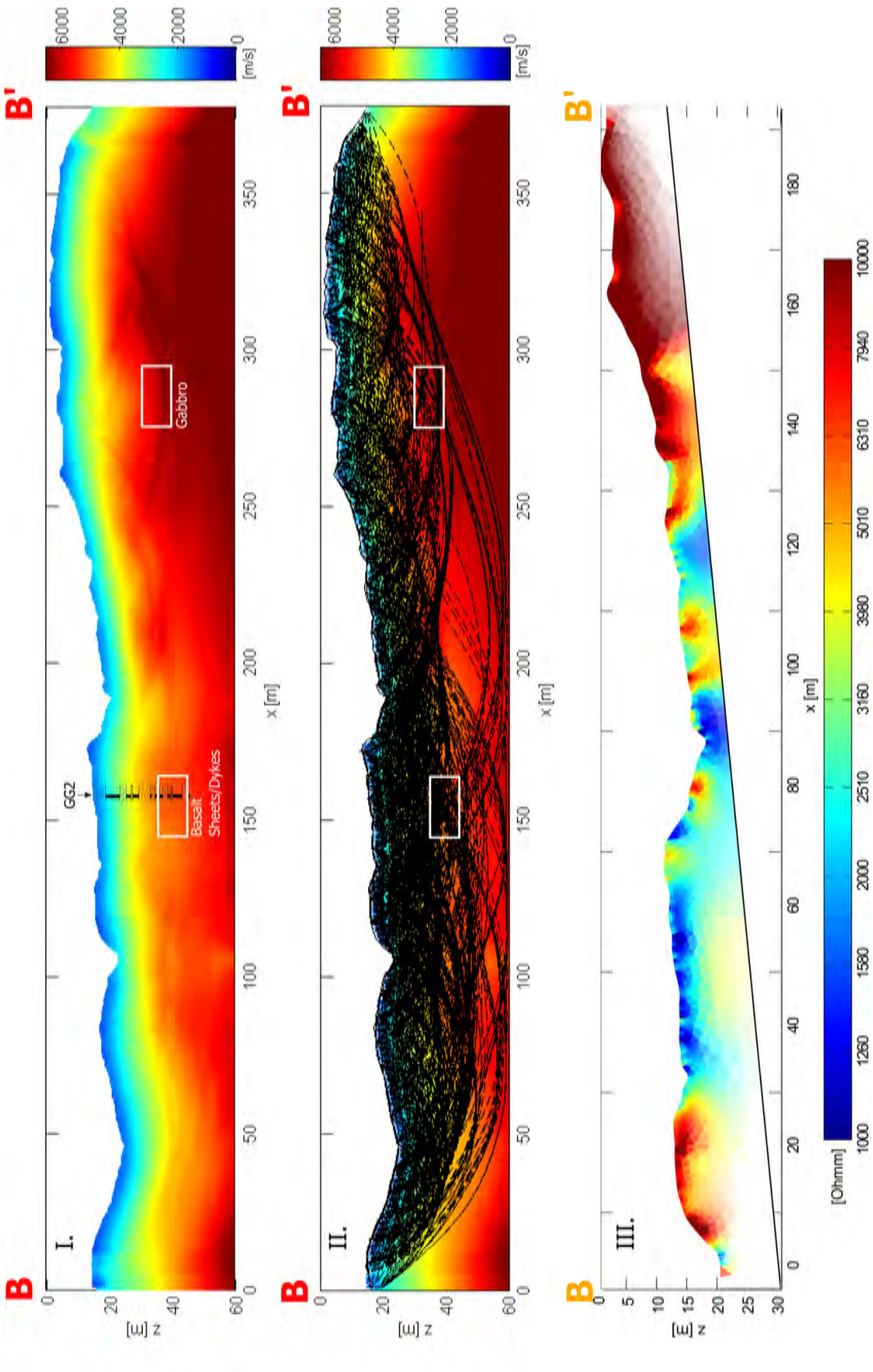

Figure 33: Results from line B. I. shows the P-wave velocity model (RMS error: 1.9 ms). II. shows the ray coverage. III. is the subsurface resistivity model (RMS error: 26.6 %). The white boxes show the area where typical values for basalt and gabbro were extracted.

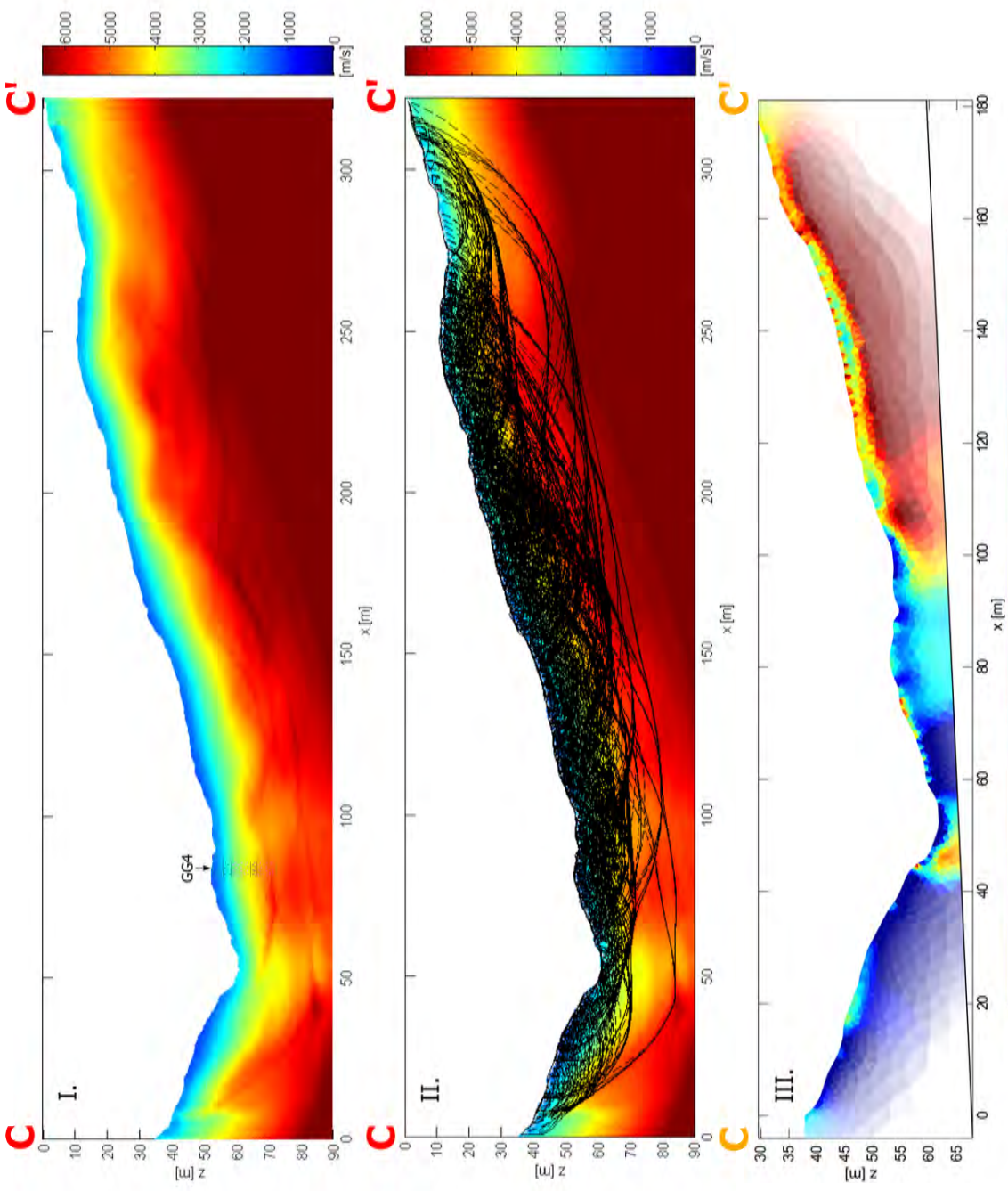

Figure 34: Results from line C. I. shows the P-wave velocity model (RMS error: 2.1 ms). II. shows the ray coverage. III. is the subsurface resistivity model (RMS error: 20.1 %).

4.1.1 Bore hole information from the IMAGE project

Core drillings were carried out in May 2014 at several places close to the measured geophysical profiles as a part of the IMAGE (Integrated Methods for Advanced Geothermal Exploration) project. The resultant geological logs are shown in Figure 35. None of the wells drilled into the gabbro, hence a clear contact zone cannot be seen in the logs. But the logging showed that host rock, dykes and sheets alternate randomly. It seems the rocks in the well close to line C consist mostly of dykes and sheets and maybe some gabbro. This might be an indication that the well was close to the contact zone or at least in an area consisting of intrusions.

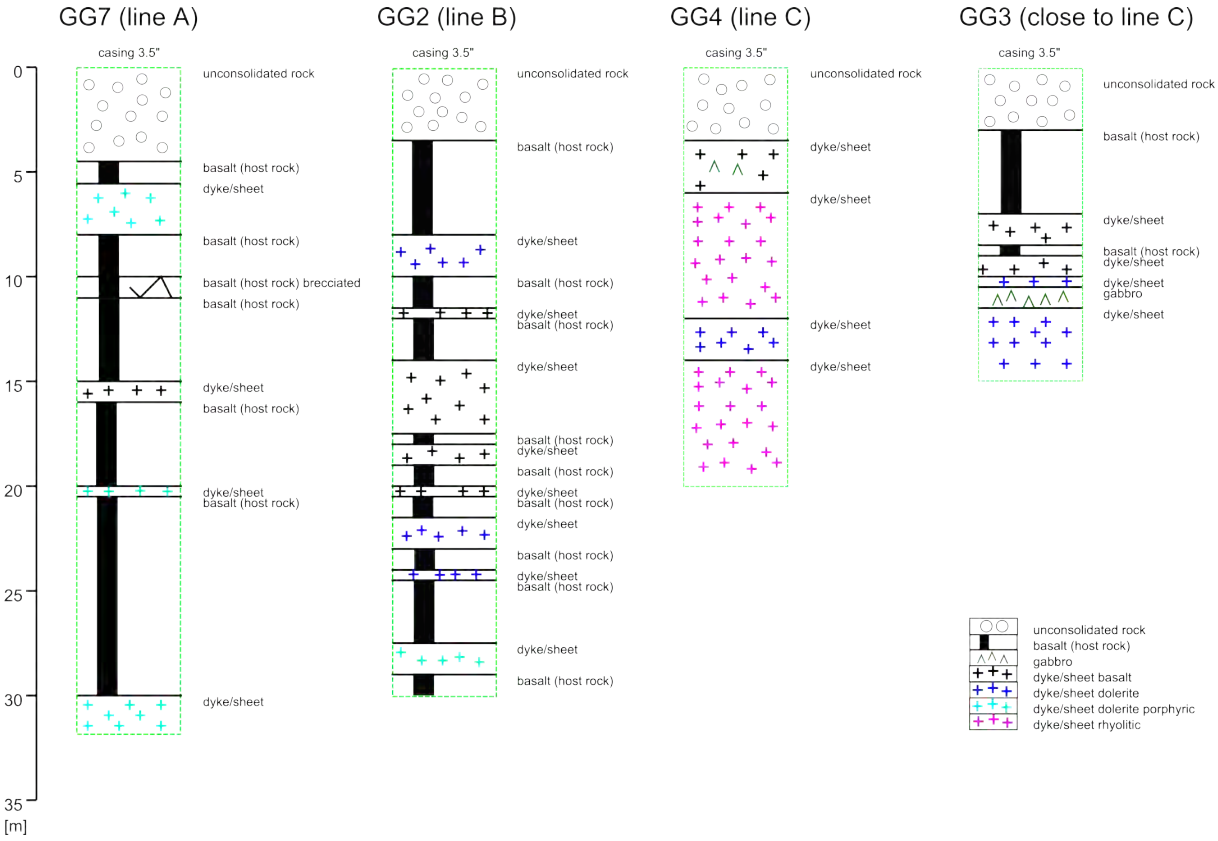

Figure 35: Well logging sheet from boreholes close to the measured geophysical lines at Geitafell. Original information at the drilling (May 2014) was written up by Omar Fridleifsson but slightly modified here (personal communication).

4.2 Subsurface models at Hoffell (Profiles X, Y and Z)

The principal expected difference in the rocks from the three profiles at Hoffell is their degree of alteration. But this attribute is unfortunately not the only one because each lava flow has also its own characteristics (differences in grain size, numbers of vesicles etc.).

The subsurface velocity models derived from lines X and Z exhibit a similar velocity range. However, the velocity model from line X has an area where velocities are lower. This variation could be the result of an intersecting dyke. Such a dyke has been mapped in the field during the measurements at approximately this location. The dyke has its orientation perpendicular to the profile and this prominent border (fractures) could lead to a zone with lower velocity. The velocity model obtained for line Y shows similar velocities but some areas have slightly lower velocities. A summary of the P-wave velocity ranges extracted from the velocity models at Hoffell can be found in Table 4. The criteria for selection were that the area from where the values were extracted needed to be from a certain depth (below weathered) and needed to have a good ray coverage.

The three inverted subsurface resistivity models at Hoffell show clearly how the weather conditions and therefore the soggy and saturated soil influenced the measurements/models. The only model (line X) which shows a resistive upper most part is the one where measurements were carried out under dry conditions. The moisture might also affect the deeper parts of the model because it shows slightly higher resistivity values than the other profiles taken under wet conditions. A comparison of the extracted resistivity values of the three profiles is given in Table 4. Only values which were not directly affected by the weather conditions were used.

To summarise, no direct and clear relation between the alteration and the elastic/electric properties can be seen. And only ranges of velocities/resistivities can be extracted instead of accurate values.

Table 4: Typical values (P-wave velocities and resistivities) extracted from the subsurface models at Hoffell.

Line	**P-wave velocities** $[m/s]$	**Resistivities** $[\Omega m]$
X	4'500 - 6'000	3'000 - 5'500
Y	4'000 - 6'000	3'000 - 5'000
Z	4'500 - 6'000	3'000 - 5'000

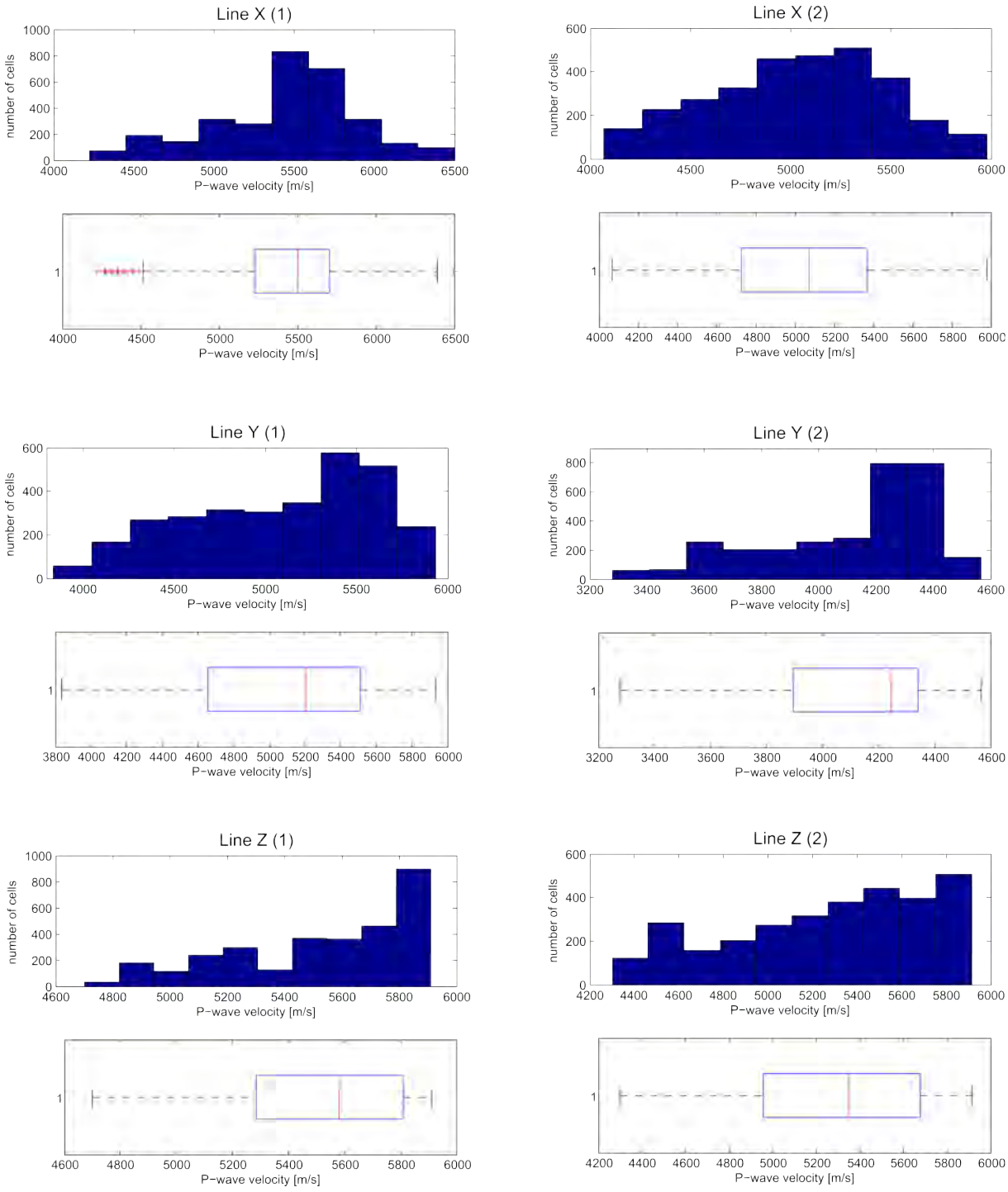

Figure 36: Histogram and boxplot of P-wave velocities from lines X, Y and Z. The values involved are taken from the areas of the white boxes shown in Figures 37, 38 and 39.

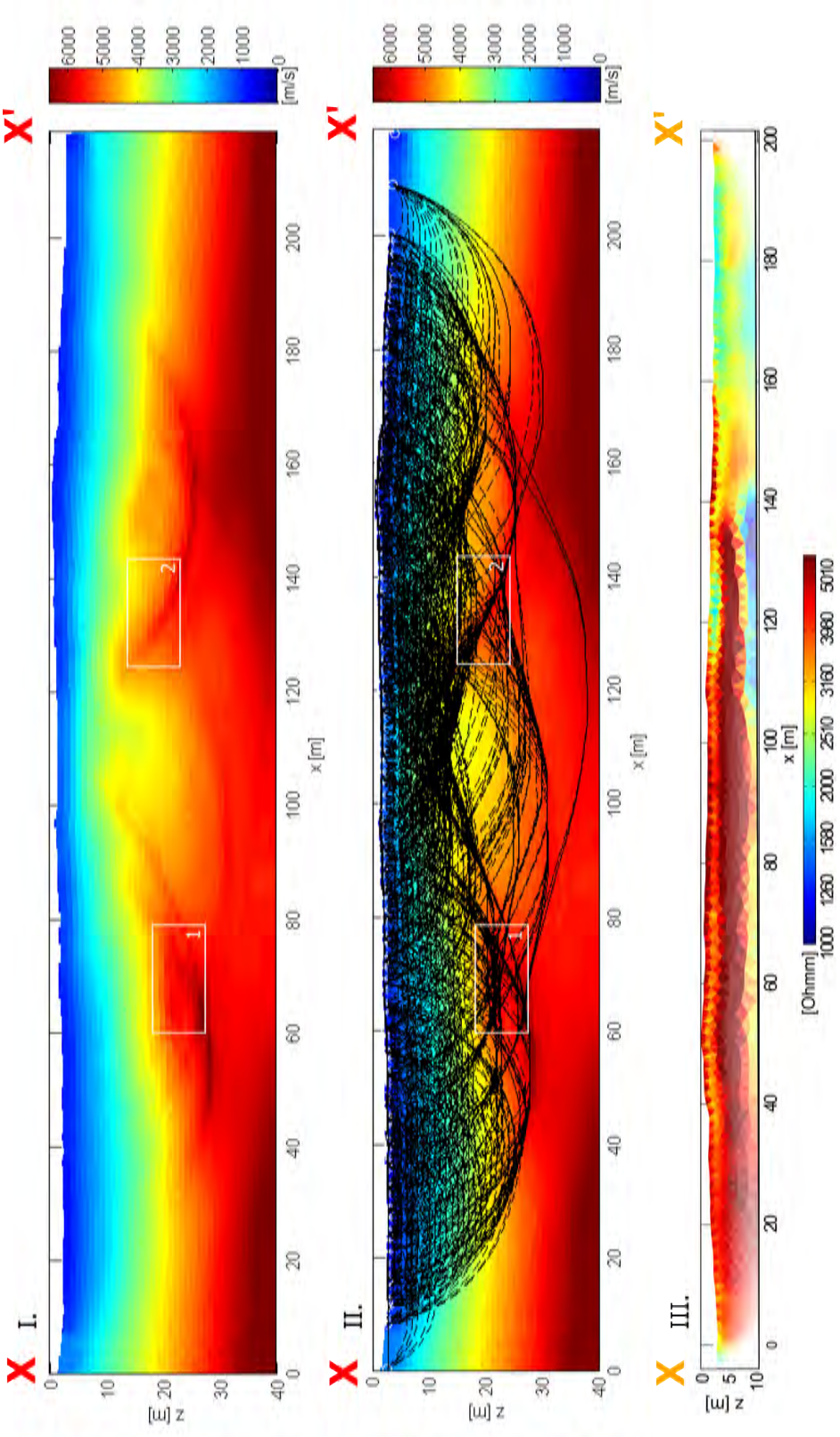

Figure 37: Results from line X. I. shows the P-wave velocity model (RMS error: 1.8 ms). II. shows the ray coverage. III. is the subsurface resistivity model (RMS error: 19.4 %). The white boxes show the area where typical values were extracted.

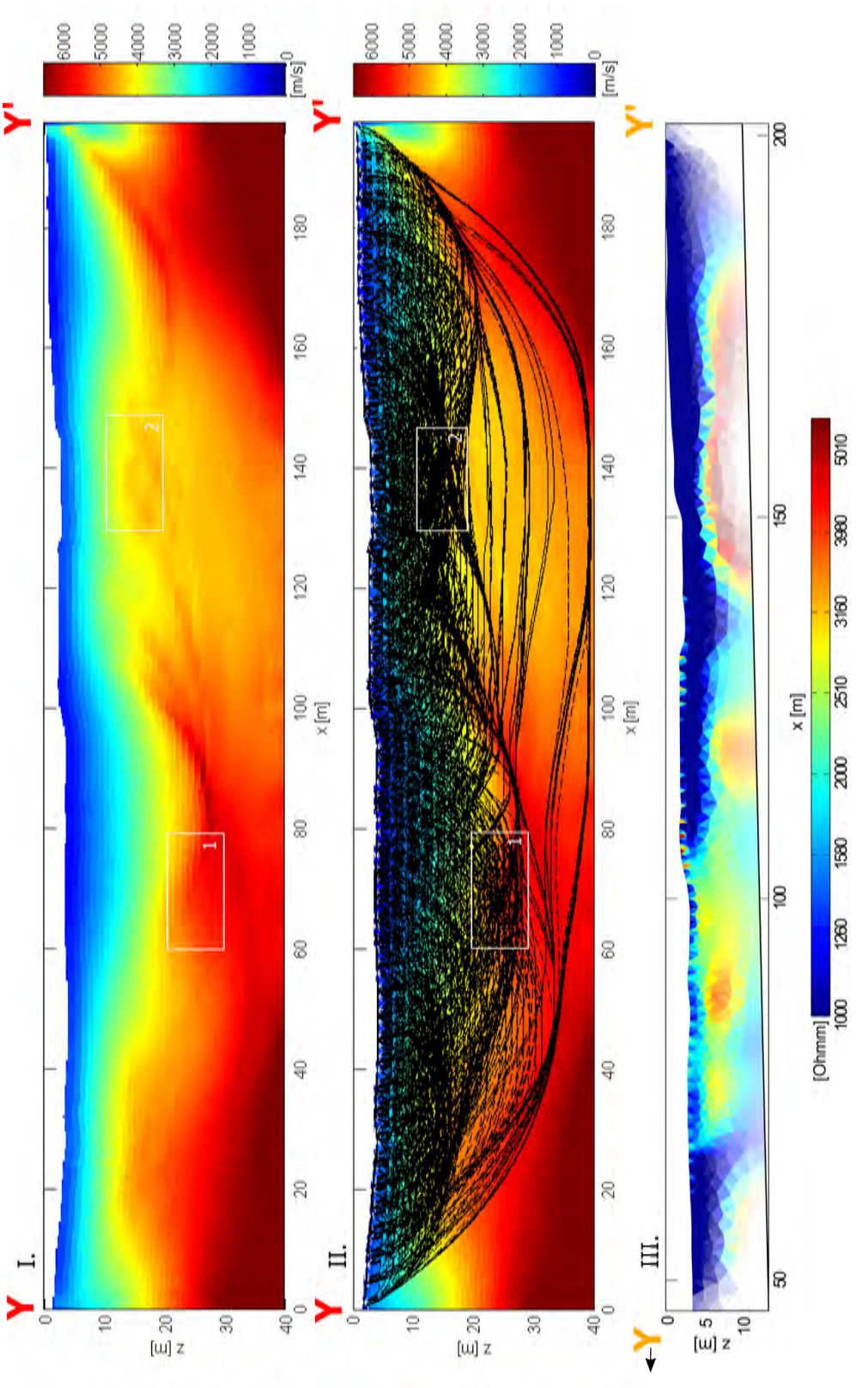

Figure 38: Results from line Y. I. shows the P-wave velocity model (RMS error: 2.0 ms). II. shows the ray coverage. III. is the subsurface resistivity model (RMS error: 12.0 %). The white boxes show the area where typical values were extracted.

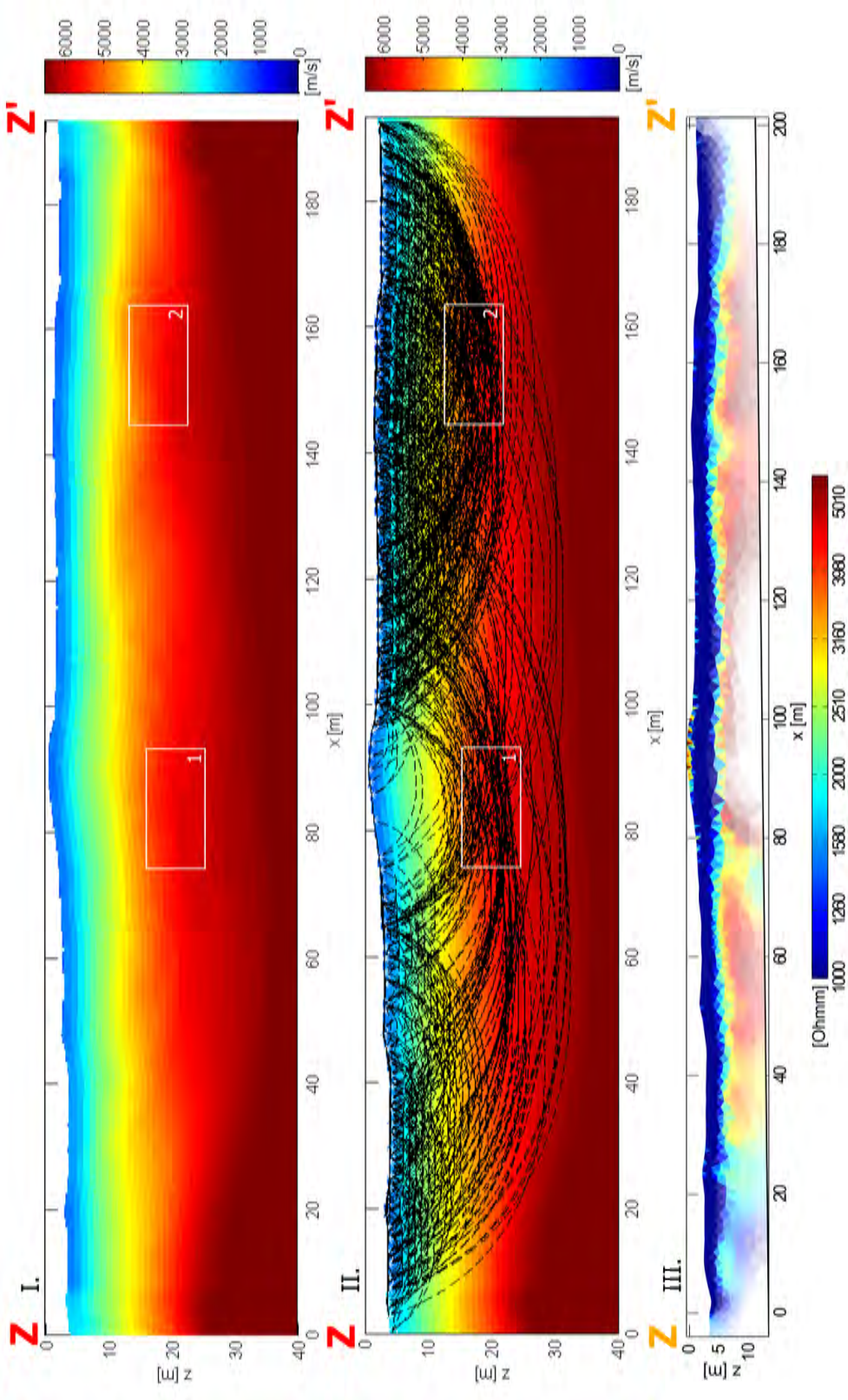

Figure 39: Results from line Z. I. shows the P-wave velocity model (RMS error: 1.4 ms). II. shows the ray coverage. III. is the subsurface resistivity model (RMS error: 12.0 %). The white boxes show the area where typical values were extracted.

4.3 Lab measurements

The rock samples collected from the field site in Iceland were examined in the Rock Physics lab at ETH Zurich. Our main interest was in the P-wave velocities. They were classified into four different groups (dependent on rock type/conditions) for comparison purposes, each examining a different aspect. Figure 40 shows these four diagrams of measured P-wave velocities as a function of confining pressure (10-250 MPa). A linear regression was then carried out on each curve between pressures of 100 and 250 MPa to be able to extract the velocity Vp_0 at normal pressure. This is the intercept of the linear fit with the zero pressure axis shown by the coloured boxes on the velocity axis. All calculated velocities and other properties of the measured rocks in the lab are listed in Table 5.

Figure 40a shows the velocities of the four main rocks. Gabbro has the highest velocity followed by the dolerite rock sample. Basalt and hornfels seem to have a slightly lower velocity. This trend is probably due to the higher density of the rocks towards lower velocity or it might also be the effect of microcracks at the borders of the minerals. If the size of the minerals gets smaller, more microcracks appear.

Basalt velocities can vary substantially (dependent on rock conditions) and this is shown in Figure 40b and 40c. There are several factors responsible for the variability. All rocks involved have more or less the same chemical composition. But the minerals were crystallised over a different time scale, experienced a different level of alteration (build-in secondary minerals differ) or have different sizes and numbers of vesicles. Lava flows slightly differ from each other and this makes it difficult to find a representative sample. But it can be seen that the basalt from the actinolite zone has the highest velocity, followed by the basalt from the epidote zone and finally the basalt from the garnet zone. Hence, we cannot establish a trend that would suggest a decrease of P-wave velocity with decreasing alteration (decreased temperature during the time the hydrogeothermal system was active). Differences are rather caused by the mineral size or the porosity of the rock. But the differences can also be explained by the fact that the rock samples from the epidote and garnet zones are more weathered than the rock samples from the actinolite zone.

Figure 40c shows that vesicles can also have an influence on the velocities of the rock samples. The basalt with no vesicles present has the highest velocity. The others vary over a range of about 1'000 m/s. It might be that the shape and size of the vesicles play an important role. Some vesicles might have a more stable shape than others, hence a

higher velocity.
Besides basalts, dolerite velocities can also vary a lot. Three samples and their measured velocities are shown in Figure 40d. It seems that the size of the minerals has an effect on the P-wave velocities with an increase in velocity with larger mineral sizes.
To summarise, gabbro has the highest velocity wavespeed, followed by dolerites. But they vary over a range of about 500 m/s. Also, basalts seem to vary in their P-wave velocity over a range of about 1'000 m/s depending on other characteristics. It seems the smaller the mineral size the lower the P-wave velocity.

Table 5: P-wave velocity results from lab measurements categorised into four parts according to rock type and rock condition. Vp0 velocity values were calculated from a linear regression of data points from 100 to 250 MPa.

	Rock sample	**Porosity** [%]	**Rock density** $[kg/m^3]$	**Matrix density** $[kg/m^3]$	**Vp0** $[m/s]$
(a)	Gabbro	2.97 ±0.24	2840 ±7	2927 ±1	6478 ±4
	Dolerite	3.46 ±0.08	2907 ±2	3011 ±1	6366 ±2
	Hornfels	2.59 ±0.04	2758 ±0	2831 ±1	5474 ±12
	Basalt	3.72 ±0.08	2975 ±2	3090 ±1	6141 ±5
(b)	Basalt actinolite zone	3.72 ±0.08	2975 ±2	3090 ±1	6141 ±5
	Basalt garnet zone	1.20 ±0.09	2967 ±2	3003 ±1	5986 ±16
	Basalt epidote zone	2.71 ±0.08	2745 ±2	2821 ±0	5989 ±9
(c)	Basalt with no vesicles	3.72 ±0.08	2975 ±2	3090 ±1	6141 ±5
	Basalt with few vesicles	3.25 ±0.16	2710 ±4	2801 ±1	4968 ±14
	Basalt with many small vesicles	2.71 ±0.08	2745 ±2	2821 ±0	5989 ±9
	Basalt with many big vesicles	3.01 ±0.09	2703 ±2	2787 ±1	5428 ±11
(d)	Dolerite aphyric 1	3.86 ±0.08	2839 ±2	2953 ±1	5891 ±15
	Dolerite aphyric 2	3.46 ±0.08	2907 ±2	3011 ±1	6366 ±2
	Dolerite porphyric	3.31 ±0.08	2839 ±2	2937 ±0	6413 ±9

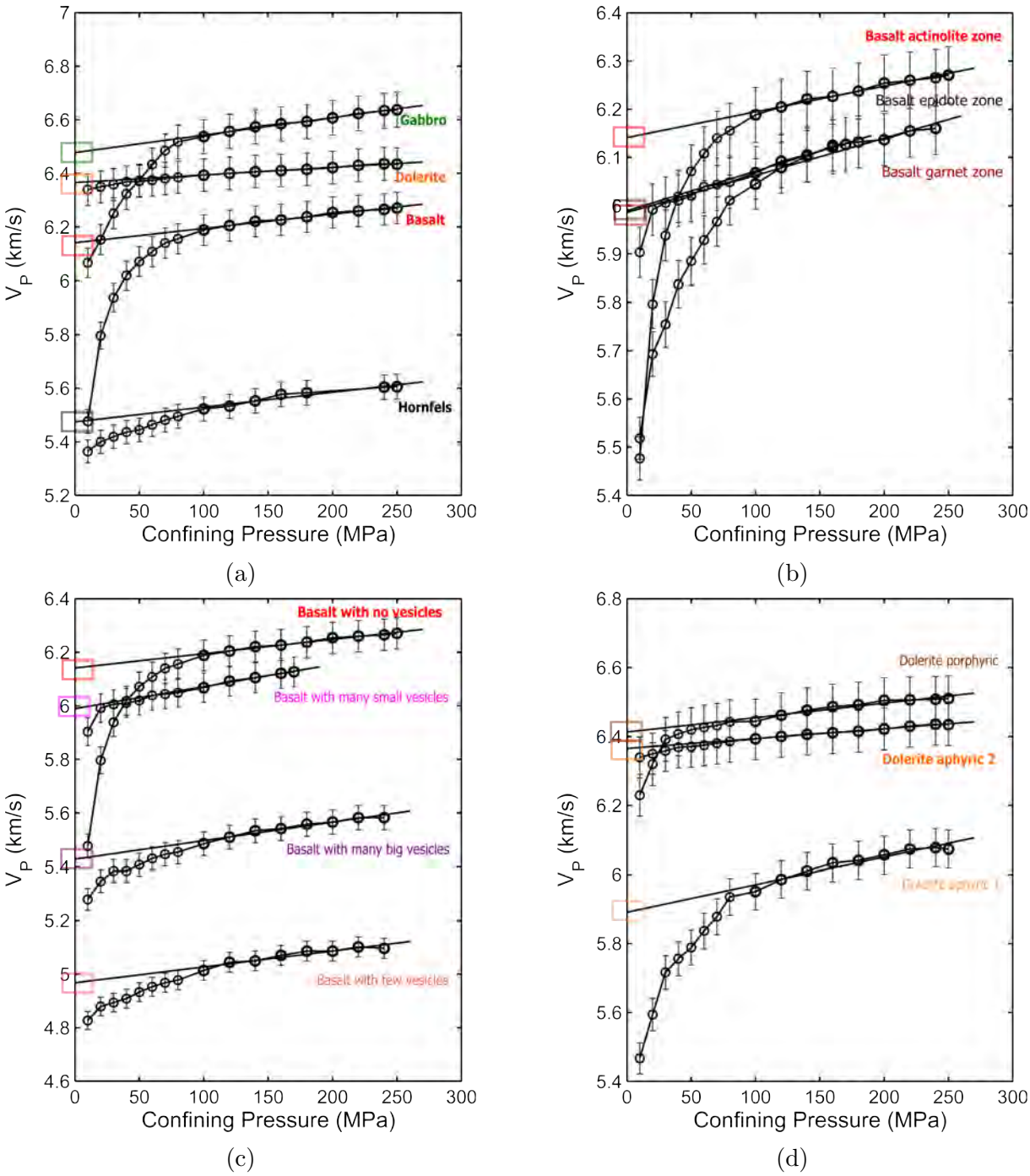

Figure 40: P-wave velocity results from lab measurements. The coloured boxes show the velocities Vp_0. These values represent the P-wave velocities of the rocks at zero pressure with closed cracks. (a) The four main rock samples (gabbro, dolerite, hornfels and basalt). (b) Rock samples (basalt) from different alteration zones. (c) Rock samples (basalt) with a different number and size of vesicles present. (d) Different types of dolerites.

5 Discussion

5.1 Field campaign, data quality and inverse modeling

The field campaign passed without major problems or interruptions at Geitafell in Iceland in August and September, 2013. Reconnaissance as well as small-scale geological mapping was carried out by David Baumann and myself. Geophysical field measurements (DC electric and seismic) were conducted at six separate locations and afterwards we collected representative rock samples as well. The samples were chosen so that each lithological unit and characteristic samples were present.
Bad weather, including windy and rainy days, influenced the data quality to an extent but most of the measurements planned were able to be carried out. The field site was remote from civilization in a rural area close to the glacier Hoffelljokull, and so cultural noise was low. Data quality suffered more from difficulties which occurred from poor contact between geophones/electrodes and the ground, or from difficulties of transferring all the energy of the seismic source into ground due to the surface conditions where it was sometimes not that easy to drill a hole deep enough for the shotgun.
Pre-processing of the data started shortly after the survey. The measured raw data had to be turned into a format which could be used afterwards. This meant that data needed to be filtered and supporting information such as topography was added to the files. An initial examination of the data gave a first impression of data quality and hints to handle further processing steps. Several different approaches were tested during processing but it was decided to apply rather high smoothing to all subsurface models (P-wave velocity and resistivity) during the inversion. The reasons are that the inverse problem was severely under-determined and we were really only interested in large-scale variations to characterise the in-situ fresh rock velocities.

5.2 Comparison of seismic field data to seismic lab data

Seismic velocities obtained from the lab data are in general higher than the values measured in the field, mainly due to the application of much higher frequencies in the lab. Frequencies around 100kHz-1MHz are used in the lab whereas in the field the frequency is only 10-100Hz. There is generally some velocity dispersion present in material media due to visco-elasticity, which leads to higher velocity at higher frequency [Mavko et al., 2009]. Moreover the lab samples are intact specimens, free of defects and cracks/joints which

can lower the in-situ velocities. Besides the different frequencies also the scale on which the measurements were taken are completely different. Lab measurements concentrate on the really small-scale features such as the small cracks, grain size, porosity and secondary inclusions while larger scale features such as weathered rocks, faults and larger geological boundaries have an impact on the field measurements.
Both measurements showed that the rock velocities can vary over a certain range. Different basalts have a velocity range in the lab measurements of about 1'300 m/s (4'900 m/s - 6'200 m/s) whereas the velocity range from the field measurements is about 600 m/s (4'700 m/s - 5'300 m/s). Hence the field measurements have slightly lower velocities as expected. This holds true also for gabbro. Field measurements indicated a velocity of about 6'000 m/s while a P-wave velocity of about 6'500 m/s was measured in the lab.
To summarise, the P-wave velocities measured in the lab are about 5-10 % higher than those measured in the field, but otherwise agree with each other quite well. The rather small differences would also imply that the measured velocity values in the field are not appreciably affected by fractures and other large-scale defects.

5.3 Geochemical composition of the rock samples

All rocks found at the field site have basically the same chemical composition (Masterthesis of David Baumann: Alteration and petrology in a fossil hydrothermal system at Geitafell central volcano, Iceland, 2014). The rock samples consist mostly of the minerals pyroxene (augite; 40-60%), plagioclase (labradorite; 40-60%) and ilmenite (5-7%). Several secondary minerals can be find as well in the rocks but only in minor amounts ($< 1\%$; actinolite, garnet, epidote, chlorite, quartz, calcite, pyrite and zeolite). They replace the mineral pyroxen in most cases or are formed in veins and vesicles.
Figure 41 shows the chemical composition of some rocks collected in the field. Only the gabbro seems to have a slightly lower SiO_2 content than the others, but otherwise all rocks are located in the same part of the plot.

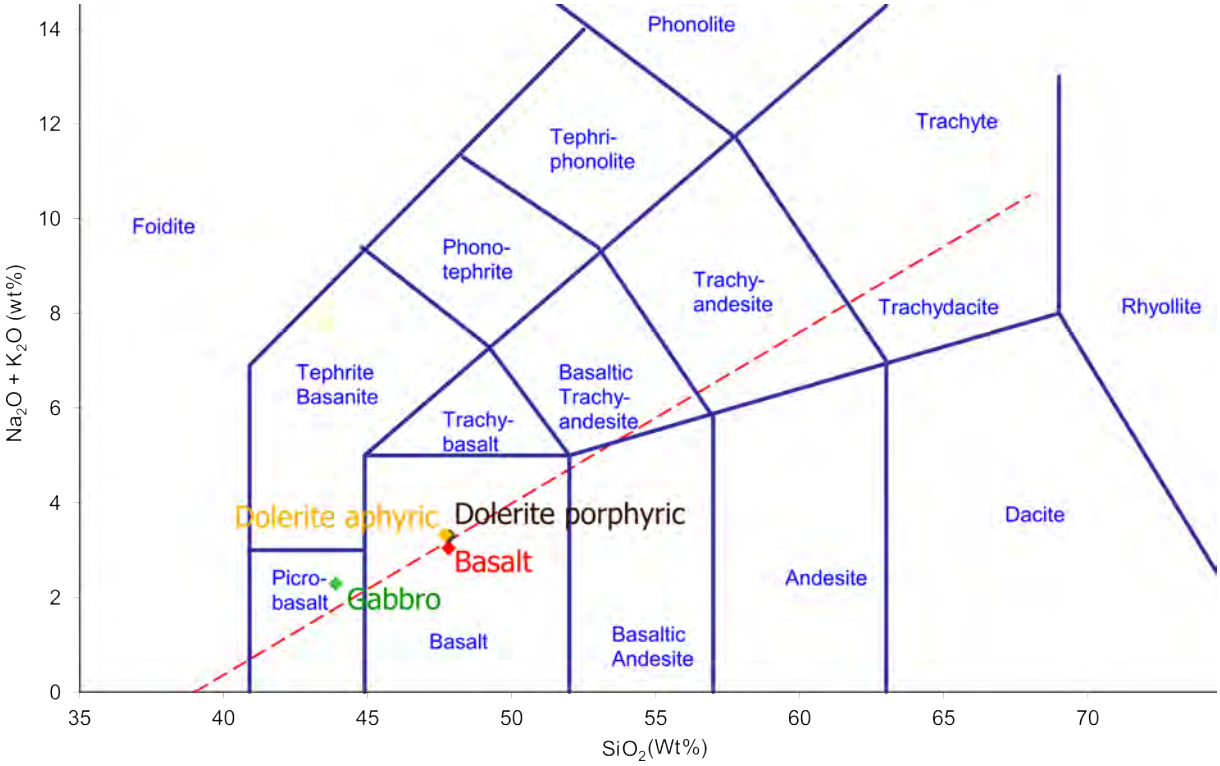

Figure 41: Total alkalis vs. silica diagram of rock samples collected at the geophysical sites in Geitafell (XRF measurements done by David Baumann, personal communication).

5.4 Comparison to other measured petrophysical properties

Christensen and Wilkens [1982] did seismic measurements on rock samples from a borehole near Reydarjoerdur, which is around 80 km north-east of Geitafell. Their velocities are in the same range as ours and they showed that with low porosity (like in our rock samples) the velocity can indeed be that high.

The grade of alteration and therefore which minerals will be replaced and built-in depends of course on the temperature but the rock alteration (number of replaced minerals) in basaltic lavas is also related to the porosity [Franzson et al., 2001]. All our rock samples showed a very low porosity ($< 4\%$) and therefore alteration minerals exist in minor amounts ($< 1\%$). Franzson et al. [2001] found that lower density alteration minerals replace the high-density primary minerals at first and therefore the mean grain density decreases with increasing alteration (increasing temperature). And later on for the chlorite zone, epidote zone and higher alterations (higher temperature), density increases again due to the growth of higher density minerals. But the effect of alteration on the

velocities is rather small in our rock samples due to the low porosity and therefore the low amount of secondary minerals. The differences in velocity in our rock samples could be more likely due to grain-boundary microcracks which can lower the velocity [Franzson et al., 2001].

Resistivity measurements at high-temperature hydrogeothermal systems were carried out by Árnason et al. [2000]. They found a low resistivity cap (mainly due to clay alteration and the more conductive surface/bulk) at the outer margins which is underlain by a more resistive core towards the inner part. Our measurements were on a fossilised high-temperature system which did not include the low resistivity cap (low alteration secondary minerals). The more resistive core towards the inner part can be confirmed by our measurements by the observed general trend of increasing resistivity towards the old magma chamber.

6 Conclusions and Outlook

Geophysical measurements (DC electric and seimsic) were carried out at six locations in Geitafell (in the south-east of Iceland) in September 2013. Their analysis yield information about resistivities and P-wave velocities of several lithological units in a fossilised high-temperature hydrogeothermal system. Therefore, velocity values (or at least ranges of velocities) could be found for the rock types such as gabbro, basalt, dolerite and hornfels. Representative values were extracted from that part of the subsurface where ray coverage was good enough and depth was sufficient to ensure unweathered material. Seismic lab measurements of collected rock samples from the same sites showed similar ranges of velocities but were about 5-10% higher due to the use of higher frequencies and a different length scale during the measurements. Other lab measurements showed that the chemical composition of the rocks is nearly the same everywhere; the variations are only minor. An exact boundary between the old magma chamber (gabbro) and the surrounding host rock (basalt) could not be imaged in the subsurface models due to the rather poor data quality (and attendant use of a high smoothing of the models and low resolution). But at least a general trend of increasing resistivity/P-wave velocity towards the gabbro can be seen. The relation between alteration and petrophysical properties could also not be resolved clearly.

More accurate and more precise field data could be achieved with some improvements in acquisition such as using a more powerful source (for both seismics and DC electrics) or enhancing the data quality by drilling more holes where better contact between the ground and the geophones/electrodes is ensured. To enhance the resolution the electrode/geophone spacing could be shortened by a factor of two. It also would be helpful to have more reliable systems in the field. The experience gained to date in this type of data under such conditions could probably also be used to get even better results (subsurface models).

The lab measurements need to be upscaled now and translated into an active geothermal system i.e. extrapolated to prevailing conditions. The petrophysical properties will change due to the higher temperature and pressure plus different fluid content. These factors will have a major impact on the measured values. Such extrapolated values will be more realistic for an active high-temperature hydrogeothermal system. Later on, all collected information will be used for numerical modeling studies to predict the expected geophysical responses, and link these with reservoir dynamics.

7 Acknowledgements

I would like to thank Melchior Grab, PhD student at ETH Zuerich, for his effort organising the field trip to Iceland and helping doing fieldwork; for being a provider of tips and tricks or just being there and always a helpful person. I would also like to thank Stewart Greenhalgh and Hansruedi Maurer for being there, whenever I had questions. Thomas Driesner, Gudmundur Ómar Fridleiffson and Knútur Árnasson made a memorable and fantastic introduction to the field area in Iceland. Sincere thanks are given to them all. But without helpers during the field work, none of this would have been possible, therefore a special thanks to Mykola Khyzhnyak and Telma Dís Sigurdardóttir for their enthusiastic participation. Last but no least I need to mention and thank David Baumann, Geochemistry Master student, who also is involved in the project. I didn't want to miss his work during the field days and the discussions about the geology of the field area. Thanks a lot!

References

M Adelinet, J Fortin, Y Guéguen, A Schubnel, and L Geoffroy. Frequency and fluid effects on elastic properties of basalt: Experimental investigations. *Geophysical Research Letters*, 37(2), 2010.

Knútur Árnason, Ragna Karlsdóttir, Hjálmar Eysteinsson, Ólafur G Flóvenz, and Steinar Thór Gudlaugsson. The resistivity structure of high-temperature geothermal systems in Iceland. In *Proceedings of the World Geothermal Congress 2000, Kyushu-Tohoku, Japan*, pages 923–928, 2000.

Knútur Árnason, Hjálmar Eysteinsson, and Gylfi Páll Hersir. Joint 1D inversion of TEM and MT data and 3D inversion of MT data in the Hengill area, SW Iceland. *Geothermics*, 39(1):13–34, 2010.

Stefán Arnórsson. Geothermal systems in Iceland: Structure and conceptual modelsI. high-temperature areas. *Geothermics*, 24(5):561–602, 1995.

S Burchardt and A Gudmundsson. The infrastructure of Geitafell volcano, southeast Iceland. *Studies in Volcanology: The Legacy of George Walker, Spec. Publ. of IAVCEI*, 2:349–370, 2009.

Steffi Burchardt, David C Tanner, Valentin R Troll, Michael Krumbholz, and Ludvik E Gustafsson. Three-dimensional geometry of concentric intrusive sheet swarms in the Geitafell and the Dyrfjöll volcanoes, eastern Iceland. *Geochemistry Geophysics Geosystems*, 12(7):Q0AB09, 2011.

Nikolas I Christensen and Roy H Wilkens. Seismic properties, density, and composition of the Icelandic crust near Reydarfjördur. *Journal of Geophysical Research: Solid Earth (1978–2012)*, 87(B8):6389–6395, 1982.

T Driesner. COTHERM - COmbined hydrological, geochemical and geophysical modeling of geoTHERMal systems. 2012.

A Elders. Iceland Deep Drilling Project (IDDP): Arsenic Distribution and Mobility in Active and Fossil Geothermal Systems in Iceland. 2010.

Wilfred A Elders and Gudmundur Ó Fridleifsson. The Science Program of the Iceland Deep Drilling Project (IDDP): a study of supercritical geothermal resources. In *Proceedings of the World Geothermal Congress. Bali Indonesia*, pages 25–29, 2010.

Hjálmar Eysteinsson and John F Hermance. Magnetotelluric measurements across the eastern neovolcanic zone in south Iceland. *Journal of Geophysical Research*, 90(B12): 10093–10, 1985.

ÓG Flóvenz, Erik Spangenberg, Johannes Kulenkampff, Knútur Árnason, Ragna Karlsdóttir, and Ernst Huenges. The role of electrical interface conduction in geothermal exploration. In *Proc. World Geothermal Congress, Antalya, Turkey*, 2005.

J Fortin, S Stanchits, S Vinciguerra, and Y Guéguen. Influence of thermal and mechanical cracks on permeability and elastic wave velocities in a basalt from Mt. Etna volcano subjected to elevated pressure. *Tectonophysics*, 503(1):60–74, 2011.

Hjalti Franzson, S Gudlaugsson, and G Fridleifsson. Petrophysical properties of Icelandic rocks. In *Proceedings of the 6th Nordic Symposium on Petrophysics, Trondheim, Norway*, 2001.

G. Ó. Fridleifsson. *The geology and the alteration history of the Geitafell central volcano, southeast Icleand*. PhD thesis, University of Edinburgh, 1983a.

G. Ó. Fridleifsson. Mineralogical evolution of a hydrothermal system. *Geothermal Resources Council*, Transactions Vol. 7:147–152, 1983b.

G. Ó. Fridleifsson. Mineralogical evolution of a hydrothermal system II. Heat sources - fluid interactions. *Geothermal Resources Council*, Transactions Vol. 8:119–123, 1984.

G. Ó. Fridleifsson. Geothermal acitvity in the Geitafell central volcano. *5th Int. Symp. Water-Rock Interactions*, pages 214–217, 1986.

Melchior Grab. Presentation of Research Plan, Geophysical Modeling of Icelandic Geothermal Reservoir. 2014.

Thomas Günther and Carsten Rücker. Boundless Electrical Resistivity Tomography BERT 2–the user tutorial, www.resistivity.net. 2013.

RW Henley and Alan John Ellis. Geothermal systems ancient and modern: a geochemical review. *Earth-Science Reviews*, 19(1):1–50, 1983.

JP Hermance and LR Grillot. Correlation of magnetotelluric, seismic, and temperature data from southwest Iceland. *Journal of Geophysical Research*, 75(32):6582–6591, 1970.

Gylfi Páll Hersir, Axel Björnsson, and Laust Børsting Pedersen. Magnetotelluric survey across the active spreading zone in southwest Iceland. *Journal of Volcanology and Geothermal Research*, 20(3):253–265, 1984.

Ernst Huenges and Patrick Ledru. *Geothermal energy systems: exploration, development, and utilization*. John Wiley & Sons, 2010.

Makky S Jaya, Serge A Shapiro, Líney H Kristinsdóttir, David Bruhn, Harald Milsch, and Erik Spangenberg. Temperature dependence of seismic properties in geothermal rocks at reservoir conditions. *Geothermics*, 39(1):115–123, 2010.

Reinhard Kirsch. Petrophysical properties of permeable and lowpermeable rocks. In *Groundwater Geophysics*, pages 1–22. Springer, 2009.

Líney H Kristinsdóttir, Ólafur G Flóvenz, Knútur Árnason, David Bruhn, Harald Milsch, Erik Spangenberg, and Johannes Kulenkampff. Electrical conductivity and P-wave velocity in rock samples from high-temperature Icelandic geothermal fields. *Geothermics*, 39(1):94–105, 2010.

J Kulenkampff, E Spangenberg, O Flovenz, S Raab, and E Huenges. Petrophysical parameters of rocks saturated with liquid water at high temperature geothermal reservoir conditions. In *Proceedings World Geothermal Congress, Antalya, Turkey, paper*, volume 1610, 2005.

John Lagat. Hydrothermal alteration mineralogy in geothermal fields with case examples from Olkaria domes geothermal field, Kenya. *Short Course II on Surface Exploration for Geothermal Resources. Organized by UNU-GTP and KenGen, at Lake Naivasha, Kenya*, pages 2–17, 2007.

Eva Lanz, Hansruedi Maurer, and Alan G Green. Refraction tomography over a buried waste disposal site. *Geophysics*, 63(4):1414–1433, 1998.

W. Lowrie. *Fundamentals of Geophysics*. Cambridge University Press, 2007.

Claudio Madonna and Nicola Tisato. A new Seismic Wave Attenuation Module to experimentally measure low-frequency attenuation in extensional mode. *Geophysical Prospecting*, 61(2):302–314, 2013.

Hansruedi Maurer. Assessing systematic errors in seismic crosshole data. *Geoph. Res. Letters*, 23:2681–2684, 1996.

Hansruedi Maurer and Christian Hauck. Geophysical imaging of alpine rock glaciers. *Journal of Glaciology*, 53(180):110–120, 2007.

Gary Mavko, Tapan Mukerji, and Jack Dvorkin. *The Rock Physics Handbook: Tools for Seismic Analysis of Porous Media*. Cambridge University Press, 2009.

William Menke, Michael West, Bryndís Brandsdóttir, and David Sparks. Compressional and shear velocity structure of the lithosphere in northern Iceland. *Bulletin of the Seismological Society of America*, 88(6):1561–1571, 1998.

Sverre Planke, Eivind Alvestad, and Olav Eldholm. Seismic characteristics of basaltic extrusive and intrusive rocks. *The Leading Edge*, 18(3):342–348, 1999.

J.M. Reynolds. *An Introduction to Applied and Environmental Geophysics*. Wiley, 2011.

Günther Schoenharting. Magnetic properties of rocks from the Geitafell gabbro complex, SE Iceland. *Bull. Geol. Soc. Den*, 28:21–29, 1979.

P.-J. Shih. Simulating the in situ physical properties of the upper muschelkalk aquifer. Master's thesis, ETH Zrich, Department of Earth Sciences, 2012.

Ari Tryggvason, Ólavur G Flóvenz, et al. Three-dimensional imaging of the P-and S-wave velocity structure and earthquake locations beneath Southwest Iceland. *Geophysical Journal International*, 151(3):848–866, 2002.

A Geological map Geitafell

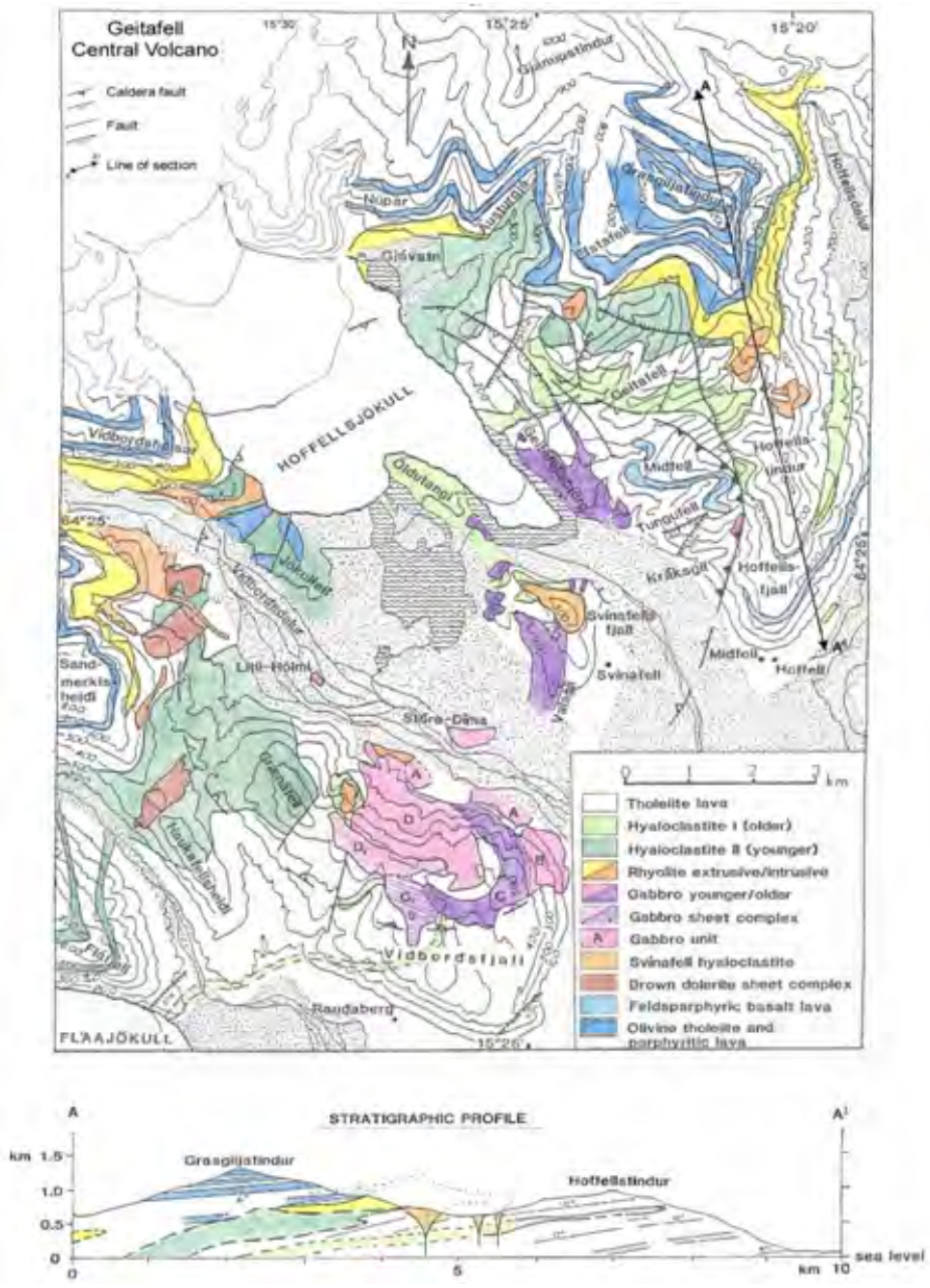

Figure 42: Geological map of the Geitafell Central Volcano in South-East Iceland. The contact zone between Gabbro and tholeiite lava can be seen at the border between the colour purple and white, [Fridleifsson, 1983a].

B Alteration zones Geitafell

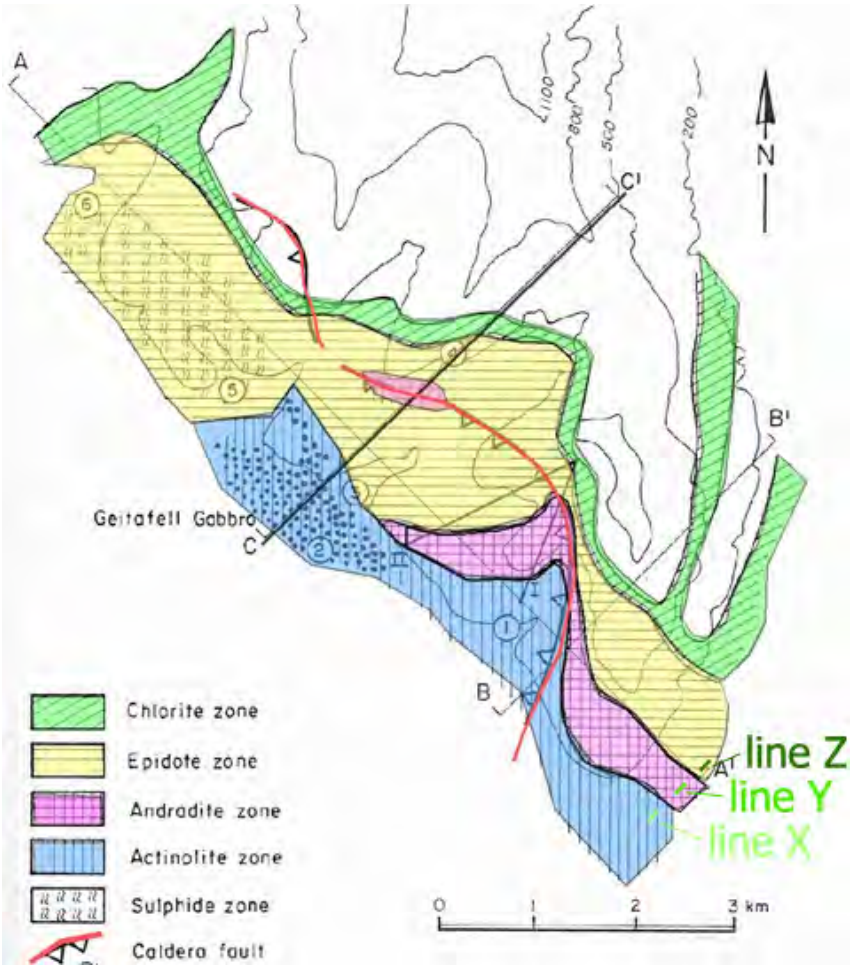

Figure 43: Alteration zones of the Geitafell Central Volcano, [Fridleifsson, 1983a]. SRT and ERT measurements (lines X, Y, Z) were carried out in September 2013 at the epidote zone, garnet (andradite) zone and actinolite zone to find out if there is a difference in the rock's (Basalt) physical parameters.

Eidgenössische Technische Hochschule Zürich
Swiss Federal Institute of Technology Zurich

Declaration of originality

The signed declaration of originality is a component of every semester paper, Bachelor's thesis, Master's thesis and any other degree paper undertaken during the course of studies, including the respective electronic versions.

Lecturers may also require a declaration of originality for other written papers compiled for their courses.

I hereby confirm that I am the sole author of the written work here enclosed and that I have compiled it in my own words. Parts excepted are corrections of form and content by the supervisor.

Title of work (in block letters):

Authored by (in block letters):
For papers written by groups the names of all authors are required.

Name(s):	**First name(s):**

With my signature I confirm that
- I have committed none of the forms of plagiarism described in the 'Citation etiquette' information sheet.
- I have documented all methods, data and processes truthfully.
- I have not manipulated any data.
- I have mentioned all persons who were significant facilitators of the work.

I am aware that the work may be screened electronically for plagiarism.

Place, date	**Signature(s)**

For papers written by groups the names of all authors are required. Their signatures collectively guarantee the entire content of the written paper.